VOL. 17 No. 5, pp. 129-160 NOVEMBER 1955

# Philips Technical Review

DEALING WITH TECHNICAL PROBLEMS
RELATING TO THE PRODUCTS, PROCESSES AND INVESTIGATIONS OF
THE PHILIPS INDUSTRIES

EDITED BY THE RESEARCH LABORATORY OF N.V. PHILIPS' GLOEILAMPENFABRIEKEN, EINDHOVEN, NETHERLANDS

## CAPACITOR MATERIALS WITH HIGH DIELECTRIC CONSTANT

by G. H. JONKER.

537.226:621.315.612:621.319.4

*In the construction of capacitors in recent years, use has often been made of ceramic materials such as $BaTiO_3$, which exhibits a very high value of the dielectric constant within a limited temperature range. It is desirable to reduce the temperature variation of the dielectric constant as much as possible, while retaining its high value. This may be done in a number of ways, such as by using mixed crystals of $BaTiO_3$ with other related compounds and by "diluting" the material with substances forming a second phase. A few examples are described here.*

### Introduction

Barium meta-titanate, $BaTiO_3$ (hereafter referred to simply as barium titanate), is a crystalline solid exhibiting the same crystal structure as the mineral perovskite ($CaTiO_3$). For rather more than ten years it has been increasingly used because of its unusual dielectric properties. It was already known that titanium dioxide ($TiO_2$) had a large dielectric constant, viz. about $\varepsilon = 114$, averaged for all crystal directions. For some compounds of titanium dioxide with other metal oxides, even larger values of $\varepsilon$ were found. Of the simple compounds, barium titanate exhibits the greatest value. This material, however, exhibits a remarkable peak in its dielectric constant-temperature curve ¹). As can be seen in *fig. 1*, the dielectric constant of barium titanate shows a very high maximum ($\varepsilon \approx 10{,}000$) at $T = 123$ °C and a slight peak at $T \approx 10$ °C. These peaks correspond to crystallographic transition points. Above 123 °C, barium titanate forms cubic crystals, between 10 °C and 123 °C, tetragonal, and below 10 °C, rhombic ²).

Below 123 °C, $BaTiO_3$ has a number of other remarkable properties which can be combined under the name "ferro-electric" properties. These are: *a*) the dielectric polarization exhibits the phenomenon of hysteresis, so that a residual polarization or remanence can occur; *b*) the dielectric constant is dependent on the amplitude of the alternating voltage used for the measurements and on the direct biassing voltage which may be applied.

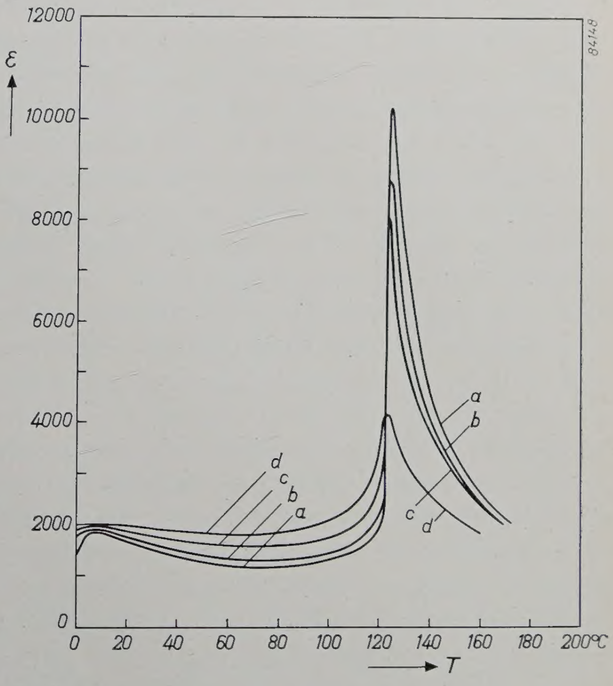

Fig. 1. The dielectric constant $\varepsilon$ of $BaTiO_3$ as a function of temperature $T$. The curves *a, b, c, d* have been measured for specimens sintered at 1400, 1350, 1300 and 1280 °C respectively. In the same order the size of the crystals decreases from about 100 μ to 5 μ. The maximum at 123 °C corresponds to the transition from cubic to tetragonal structure, the maximum at about 10 °C to the transition from the tetragonal to the rhombic structure.

---

¹) G. H. Jonker and J. H. van Santen. The ferro-electricity of titanates. Philips tech. Rev. **11**, 183-192, 1949/50; further referred to as I.

²) Below −70 °C, $BaTiO_3$ is rhombohedral. The transition point, which also gives rise to a low maximum of $\varepsilon$ (see I, fig. 4), is not shown in fig. 1.

These special properties form an obstacle to the use of barium titanate in capacitors for use in oscillators. Apart from small temperature dependence of $\varepsilon$ and low dielectric losses ($\tan \delta < 10^{-3}$), an essential requirement in this case is that the dielectric should not possess property (*b*).

The conditions are less rigid for coupling and by-pass capacitors in amplifiers and for smoothing capacitors and capacitors for interference suppression. We shall direct our attention in this article to this sort of application, for which the principal requirement is that the capacity is large in comparison with the dimensions. Variations of 10 % in both directions, resulting from temperature changes and from a voltage bias, are permissible. The dielectric losses may also be much greater ($\tan \delta < 0.03$).

Even these moderate demands cannot be met by $BaTiO_3$. In particular, the strong dependence of $\varepsilon$ on the temperature raises objections. This material only shows large values of $\varepsilon$ in a limited temperature range which, furthermore, is unfavourably situated. Fortunately it is possible to modify the properties of barium titanate in various ways. In the first place, by careful choice of the firing process, the $\varepsilon$ peak can be considerably broadened. Further, one can work, not with $BaTiO_3$, but with mixed crystals of this substance with related compounds, obtained by replacing either the Ba-ion, or the Ti-ion, or both, by analogous ions. In this way the $\varepsilon$ peak can be shifted to a more suitable temperature range, independent of the methods employed to make the peak broader. One can also "dilute" the material with another substance, either of related composition or not, which can behave as a second phase between the crystals of the original material. If the material chosen for this purpose has a smaller temperature dependence of $\varepsilon$, then the dependence on temperature of the mixture will be decreased. Finally, the properties can be favourably influenced, not only through the firing process, but by the admixture of small amounts of substances of different structure, which may dissolve in the material or settle along the crystal boundaries.

Combinations of these measures now make it possible to prepare a series of materials related to $BaTiO_3$, which do meet the requirements described above and which have been responsible for an increase in the application possibilities for materials with a large dielectric constant. We shall now consider these possibilities in more detail.

## Influencing the transition points of $BaTiO_3$

The sharp peak in the $\varepsilon$-$T$ curve for $BaTiO_3$ at $T = 123$ °C appears to be dependent on the manner of preparation of the material. For densely sintered, coarse crystalline material, with crystals of dimensions greater than 100 μ, a very high maximum is found, with a sharp drop on the lower temperature side. The graph of $\varepsilon = f(T)$ (see fig. 1, curve *a*) corresponds closely to that of a single crystal [3]).

If the material is prepared so that the crystals are much smaller, the maximum becomes lower and wider (fig. 1, curve *d* [4])). From a thorough investigation by means of X-ray diffraction photographs and from measurements of the specific heat (carried out in co-operation with J. Volger in the Research Laboratory at Eindhoven) it appears that in the ceramic material the crystallographic transition, which for a single crystal is sharply defined and takes place at a particular temperature, can be spread out over a large temperature range, e.g. between 100 °C and 170 °C. In this range one finds a mixture of two crystal forms, viz. the cubic, which is stable above 123 °C for a monocrystal, and the tetragonal, which occurs below 123 °C for a monocrystal.

That individual crystals of $BaTiO_3$ can have such divergent transition points is attributable to the fact that the transition point of $BaTiO_3$ is very sensitive to outside influences. This appears from the following thermodynamic considerations.

We start from the formula for the Gibbs free energy $G$:

$$G = U - TS + pV, \quad . \quad . \quad . \quad . \quad . \quad (1)$$

where $U$ is the energy, $S$ the entropy, $p$ the pressure and $V$ the molecular volume [5]). Since $T\mathrm{d}S = \mathrm{d}U + p\mathrm{d}V$ it follows that:

$$\mathrm{d}G = -S\mathrm{d}T + V\mathrm{d}p . \quad . \quad . \quad . \quad . \quad (2)$$

In *fig. 2* the variation of the Gibbs free energy of the cubic phase ($G_c$) and of the tetragonal phase ($G_t$) are schematically represented in the neighbourhood of the transition point. Since

$$\left(\frac{\partial G}{\partial T}\right)_p = -S,$$

the slope of these lines is determined by the entropy $S$ of the phases; the angle between the lines is determined by the difference in entropy $\Delta S = S_c - S_t$, and thus by the heat of transition

$$\Delta H = T_{ct}\, \Delta S,$$

---

[3]) W. Merz, Phys. Rev. **75**, 687, 1949.

[4]) cf. H. Kniepkamp and W. Heywang, Z. ang. Physik **6**, 385-390, 1954 (No. 9).

[5]) E.g. see J. D. Fast, Entropy in science and technology, Philips tech. Rev. **16**, 258-269 (esp. page 267), 298-308 and 321-332, 1954/55 (Nos. 9, 10 and 11).

where $T_{ct}$ is the transition temperature between the tetragonal and cubic phase.

If, by some means or another, the values of $G_t$ and $G_c$ are changed by amounts $dG_t$ and $dG_c$, which are not equal:

$$dG_c - dG_t = \Delta dG \neq 0,$$

it follows from simple geometrical considerations that the transition temperature is shifted according to the formula:

$$dT_{ct} = \frac{\Delta dG}{\Delta S} = T_{ct}\frac{\Delta dG}{\Delta H} \,. \quad . \quad . \quad . \quad (3)$$

For $T_{ct} = 396$ °K and $\Delta H = 220$ joules/mol (according to the measurements of J. Volger) we find:

$$dT = 1.8\,\Delta dG \frac{°C}{J/mol} \,. \quad . \quad . \quad . \quad . \quad (4)$$

For some external influences $\Delta dG$ is simple to calculate. Consider, for example, the effect of external pressure. If the external pressure increases by an amount $dp$, at constant temperature $T$, equation (2) becomes $dG = Vdp$, and we obtain, by substitution in eq. (3), the well-known equation of Clapeyron:

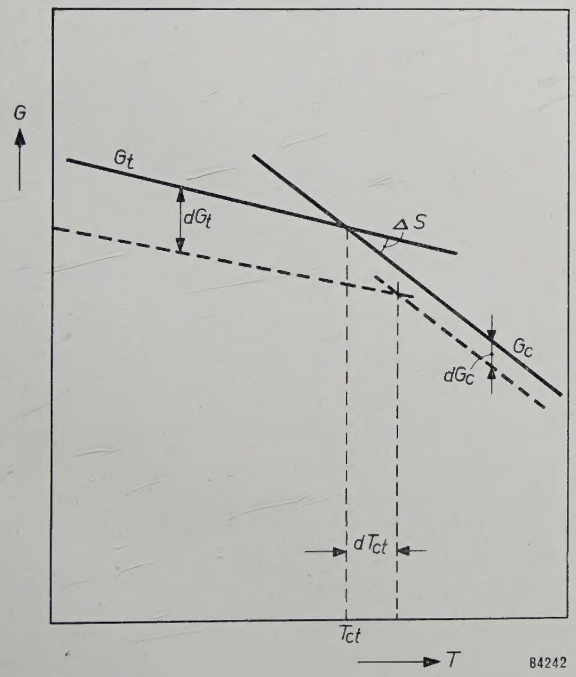

Fig. 2. Variation of the Gibbs free energy $G$ with the temperature $T$ (schematic) for cubic $BaTiO_3$ ($G_c$) and for tetragonal $BaTiO_3$ ($G_t$). The point of intersection of these lines gives the transition temperature $T_{ct}$. This point is displaced if, for any reason, the lines $G_c$ and $G_t$ are moved over different distances $dG_c$ and $dG_t$.

$$dT_{ct} = T_{ct}\frac{\Delta V\,dp}{\Delta H} \,. \quad . \quad . \quad . \quad . \quad . \quad . \quad (5)$$

The most important component of $\Delta V$ is the spontaneous change of volume at the transition point, $V_c - V_t$.

**Table I.** Dimensions of the elementary cell of $BaTiO_3$ at the transition point ($T = 123$ °C).

| | $a$ in Å | $b$ in Å | $c$ in Å | $v$ in Å$^3$ | $V$ in cm$^3$ |
|---|---|---|---|---|---|
| Cubic (c) | 4.006 | 4.006 | 4.006 | 64.288 | 38.701 |
| Tetragonal (t) | 4.000 | 4.000 | 4.021 | 64.336 | 38.730 |
| Difference (c — t) | 0.006 | 0.006 | −0.015 | −0.048 | −0.029 |

In *Table I*, $\Delta V$ is calculated from the formula $V = N_{Av}\, v$, where $v$ is the volume of the elementary cell ($v = abc$) [6]) and $N_{Av}$ is Avogadro's constant ($6.02 \times 10^{23}$/mole). With the help of these figures we find for a uniform pressure $p$:

$$\Delta T_{ct} = -5.2 \times 10^{-8}\, p \text{ °C per newton/m}^2 . \quad . \quad . \quad (6)$$

or (since 1 atm = 101,325 newtons/m$^2$), —5.3 °C per 1000 atm, which agrees fairly well with the value found experimentally by Merz [7]) for single crystals, viz. —5.8 °C per 1000 atm.

If the external pressure does not act isotropically, account must be taken of the fact that in the transition from the cubic to the tretagonal phase, the orientation of the tetragonal crystals is preferentially influenced by the direction of the external force. Equation (2), which only takes account of pressure acting in all directions, is not valid in such a case. Under uni-directional pressure a tetragonal crystal occurs with the c-axis perpendicular to the direction of the pressure. In such a case $T_{ct}$ increases as a result of the pressure so that:

$$\Delta T_{ct} = +11.2 \times 10^{-8}\, p \text{ °C per newton/m}^2 . \quad (7)$$

If the crystal be subjected to a tension, the tetragonal form is orientated so that the $c$-axis lies in the direction of the force, and $T_{ct}$ also increases [8]):

$$\Delta T_{ct} = +27.7 \times 10^{-8}\, p \text{ °C per newton/m}^2 . \quad . \quad . \quad (8)$$

For a force of 1000 kg/cm$^2$ (approx. $10^8$ newtons/m$^2$), we find $\Delta T$ to be 11 and 27 °C respectively.

It is thus clear that internal stresses, which may arise from non-uniform cooling and which may be of the order of 1000 kg/cm$^2$, can easily result in a spread of some tens of degrees in the transition temperature. It has been shown experimentally that, particularly in fine crystalline material, the spread may range from 100 °C to 170 °C.

---

[6]) For this purpose use was made of unpublished measurements by M. G. Harwood, Material Research Lab., Philips Electrical Ltd., Mitcham, England.

[7]) W. Merz, Phys. Rev. **78**, 52-54, 1950.
Compare equation (6) with that for the equilibrium of ice and water, for which $\Delta T = -8.8 \times 10^{-8}\, p$ °C/(N/m$^2$). Despite the fact that $\Delta V$ is much larger (viz. 2 cm$^3$ compared with about 0.03 for $BaTiO_3$) $\Delta T/p$ is of the same order of magnitude because $\Delta H$ is much greater for water-ice(about 6000 J/mol against 220 J/mol for BaTiO3).

[8]) See also P. W. Forsbergh, Phys. Rev. **93**, 686-692, 1954, who has found experimentally a quadratic effect for a pressure applied in two directions.

The Gibbs free energy and with it, the transition point can be influenced not only by internal stresses but also by other causes, which do not appear in equation (2). As an example of such effects, we will consider the difference in free surface energy between the tetragonal and cubic phases. It is obvious that this effect will be most strongly felt in fine crystalline material, where the total internal surface is greatest. Such material is generally obtained by sintering at as low a temperature as possible. It is then probable that the crystal growth is so incomplete that many faults occur in the lattice, which may also make a contribution to the Gibbs free energy.

From the above it is clear that by means of a combination of several measures it is possible to alter radically the $\varepsilon - T$ curve of the pure material. Further variation in the form of this curve can be obtained by making use of mixed crystals, which we shall now discuss further.

### Mixed crystals of $BaTiO_3$ with related compounds

Barium titanate forms mixed crystals with many other substances which, like itself, crystallize in the perovskite structure. Even quite small quantities of these substances affect the $\varepsilon$-$T$ curve appreciably. The effect of $SrTiO_3$ has been thoroughly studied (see I). This substance causes all three transition points to shift to lower temperatures. By the addition of $SrTiO_3$, the peak can be displaced from 123 °C to a temperature in the range in which the capacitor is to be used. For mixed crystals containing 75% $BaTiO_3$ and 25% $SrTiO_3$ for example, the main peak lies at about 50 °C.

The same is found when the Ti-ion, instead of the Ba-ion is replaced, for example, by mixing with $BaZrO_3$ or $BaSnO_3$. The zirconates and stannates shift the main peak to lower temperatures.

In such mixed crystals of $BaTiO_3$ with zirconates and stannates and other titanates, the volume change at the transition point is smaller and hence the effect of mechanical stresses is smaller. The spread at the transition point is therefore smaller and the peak in the $\varepsilon$-$T$ curve sharper 9)), at least in the case of well sintered, somewhat coarse crystalline specimens.

The desired widening and lowering of the peak must therefore be obtained by other means, such as the effect of crystal size (small crystals are favourable) and of lattice faults and inhomogeneities.

Sometimes, in the case of mixed crystals, special circumstances help in achieving the desired widening of the peak. The second transition point, which for pure $BaTiO_3$ lies at 10 °C, is shifted to higher temperatures by the addition of $BaZrO_3$ or $BaSnO_3$. For mixtures in certain proportions the first and second transition points coincide (see *fig. 3* and *4*). Mixed crystals for which the two transition points lie close together, show a broader, lower peak in the $\varepsilon$-$T$ curve.

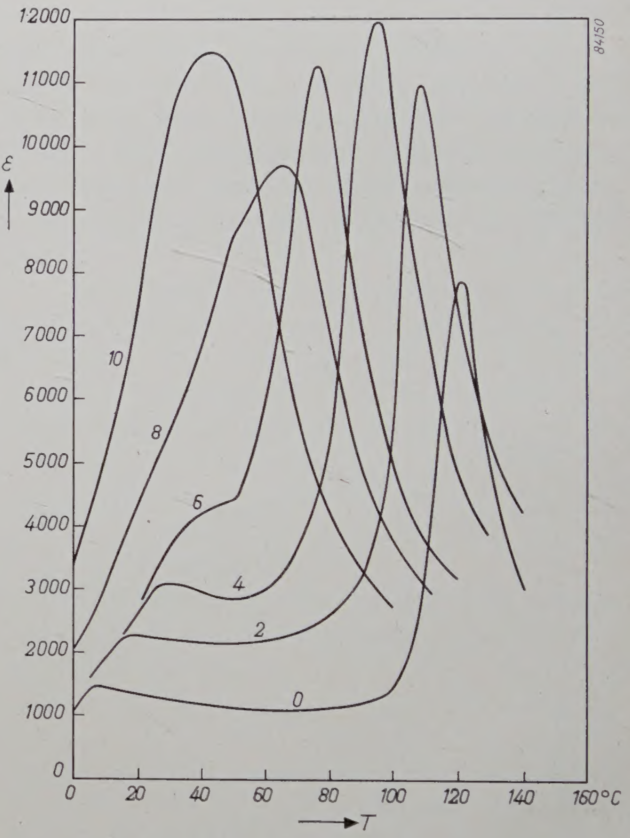

Fig. 3. $\varepsilon$-$T$ curves for mixed crystals of $BaTiO_3$ and $BaSnO_3$. The figures beside the lines give the percentage of $BaSnO_3$ present. The mixed crystals have a higher $\varepsilon$ maximum than pure $BaTiO_3$. For specimens where the first and second maxima lie close together (see fig. 4) a disturbance occurs which makes this effect less obvious.

Often when making dielectric material consisting of mixed crystals, a wide maximum in the $\varepsilon$-$T$ curve is obtained without taking any special measures to achieve this. In manufacturing these products, the basic ingredients are powdered carbonates and oxides, such as $BaCO_3$, $SrCO_3$, $TiO_2$ and $ZrO_2$. These materials have to react with each other in the solid state, for which purpose diffusion of the ions must

---

9) G. A. Smolenski, M. A. Karamyshev and K. I. Rozgachev, Doklady Akademii Nauk. S.S.S.R. **79**, 53-56, 1951.

take place. At low firing temperatures both the chemical reaction and the diffusion take place slowly, so that the formation of crystals is incomplete, resulting in small crystals, inhomogeneities and consequent widening of the $\varepsilon$-peak. This applies particularly to the case where $ZrO_2$ is present.

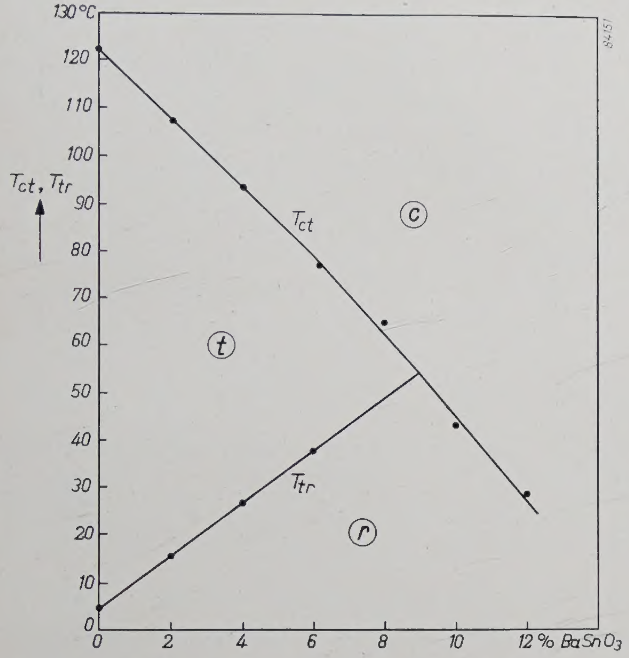

Fig. 4. The effect of $BaSnO_3$ on the transition points of $BaTiO_3$ (an almost similar figure applies for additions of $BaZrO_3$) $c$ = region of cubic structure, $t$ = tetragonal, $r$ = rhombic.

## Influence of a second phase

Another possible means of reducing the temperature dependence of the dielectric constant of the materials under discussion, is to dilute them with a substance which shows little or no variation of the dielectric constant with the temperature. A mixture of ceramic dielectrics behaves roughly according to the Lichtenecker rule of mixtures 10):

$$\log \varepsilon = v_1 \log \varepsilon_1 + v_2 \log \varepsilon_2, \quad . \; . \; . \; . \quad (9)$$

where $v_1$ and $v_2$ are the volume fractions of components with dielectric constants $\varepsilon_1$ and $\varepsilon_2$.

If the dielectric constant of the first material has the values $\varepsilon_{1a}$ and $\varepsilon_{1b}$ at temperatures $T_a$ and $T_b$ respectively, and that of the second $\varepsilon_{2a}$ and $\varepsilon_{2b}$, we then find from the rule:

$$\log \varepsilon_a = v_1 \log \varepsilon_{1a} + v_2 \log \varepsilon_{2a},$$
$$\log \varepsilon_b = v_1 \log \varepsilon_{1b} + v_2 \log \varepsilon_{2b},$$

$$\log (\varepsilon_a/\varepsilon_b) = v_1 \log (\varepsilon_{1a}/\varepsilon_{1b}) + v_2 \log (\varepsilon_{2a}/\varepsilon_{2b}). \quad (10)$$

Now if $\varepsilon$ for the second phase shows only a small dependence on $T$, so that $\varepsilon_{2a}/\varepsilon_{2b}$ differs only slightly from unity, we see that the mixing has resulted in the logarithm of $\varepsilon_a/\varepsilon_b$ being multiplied by a factor $v_1$ ($<1$), which is independent the value of $\varepsilon_2$.

It is seen from (9) that in order to achieve a large final value of $\varepsilon$, it is desirable to choose as the second phase some material which itself has a large value of $\varepsilon$. From this point of view it is fortunate that $CaTiO_3$ and $BaTiO_3$, although both crystallizing in the perovskite structure, differ so greatly in the dimensions of their elementary cells that they do not form mixed crystals in all proportions; in certain particular proportions the mixture splits into two phases, one rich and one poor in calcium. Now $CaTiO_3$ itself is a material with a fairly large value of $\varepsilon$ ($\varepsilon = 130$ at room temperature); the $\varepsilon$-$T$ curve exhibits no peaks. The temperature coefficient is negative and constant over a large range of temperatures; its value is given by:

$$\frac{1}{\varepsilon}\frac{d\varepsilon}{dT} = -1500 \times 10^{-6}\,(^\circ\mathrm{K})^{-1}.$$

The Ca-rich phase of mixed crystals of Ca- and Ba-titanate also has a constant negative temperature coefficient. The Ca-rich phase is therefore the ideal material to improve the $\varepsilon$-$T$ curve of the Ba-rich phase. This is still valid if a third substance of perovskite structure is added to shift the peak to a lower temperature. Furthermore, the remaining peak can, of course, be made wider and lower by firing at low temperatures to encourage inhomogeneity. An added advantage here is that the miscibility of Ca- and Ba-titanates decreases with decreasing temperature. During the cooling process after firing, therefore, a segregation takes place which does not lead to an equilibrium state. This produces extra inhomogeneity and internal stresses, which make the maximum of the $\varepsilon$-$T$ curve still broader.

We shall now discuss two systems in which the above-mentioned segregation plays a part.

1) The system $BaTiO_3$-$SrTiO_3$-$CaTiO_3$. This system with five components (Ba, Sr, Ca, Ti, O) is in fact a ternary system; it is restricted to compounds $MTiO_3$ with perovskite structure (M = Ba, Sr or Ca); all compositions can thus be represented graphically in a triangle with the three titanates at the corners (*fig.* 5) and each point is defined by two coordinates.

$SrTiO_3$ forms mixed crystals in all proportions with both $BaTiO_3$ and $CaTiO_3$. It crystallizes cubically with a lattice constant (3.90 Å) lying between

---

10) K. Lichtenecker, Phys. Z. **27**, 115-158, 1926.

the average values for all crystal axes of $CaTiO_3$ (3.82 Å) and $BaTiO_3$ (4.00 Å), both of which deviate slightly from cubic crystal structure. In such a case the miscibility of the original components (Ca and Ba here) usually increases as more of a third component (here Sr) is added. This in fact occurs in the present case, as may be seen from fig. 5, which shows the segregation area (two-phase area). In this region a number of straight lines have been drawn approximately parallel to the $BaTiO_3$-$CaTiO_3$ side. These are the so-called co-existence lines or connodes. The ends of each connode, lying on the boundary of the two-phase area, give the compositions of the two-phases into which a mixture, represented by a point on the connode, separates out.

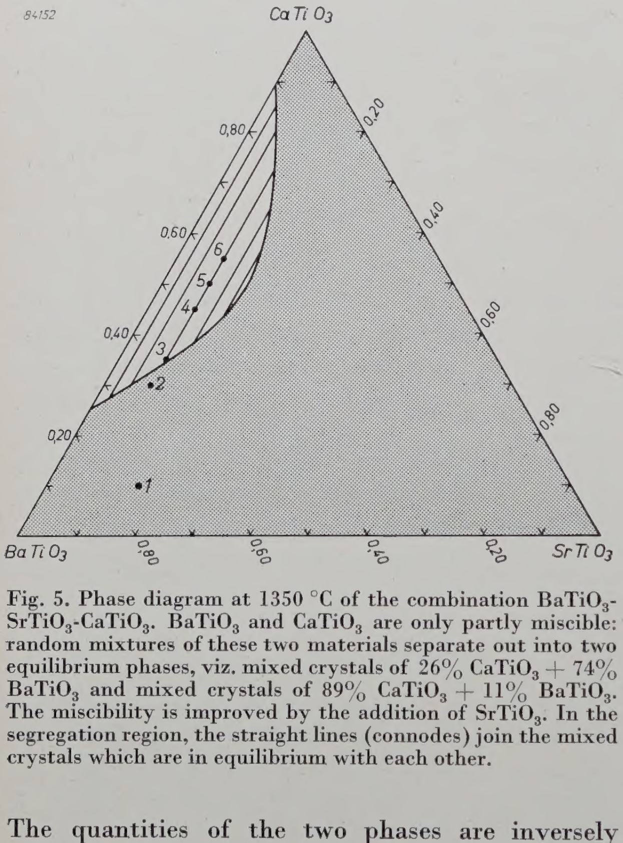

Fig. 5. Phase diagram at 1350 °C of the combination $BaTiO_3$-$SrTiO_3$-$CaTiO_3$. $BaTiO_3$ and $CaTiO_3$ are only partly miscible: random mixtures of these two materials separate out into two equilibrium phases, viz. mixed crystals of 26% $CaTiO_3$ + 74% $BaTiO_3$ and mixed crystals of 89% $CaTiO_3$ + 11% $BaTiO_3$. The miscibility is improved by the addition of $SrTiO_3$. In the segregation region, the straight lines (connodes) join the mixed crystals which are in equilibrium with each other.

The quantities of the two phases are inversely proportional to the distances of the point from the two ends of the line. A number of the mixtures studied are plotted in fig. 5, and in *fig. 6* the corresponding $\varepsilon - T$ curves are shown.

2) The system $BaTiO_3$-$CaTiO_3$-$BaZrO_3$-$CaZrO_3$. This can also be represented in a plane diagram, because only compounds with the formula $ABO_3$ occur, all of which crystallize in the perovskite structure. The number of independent variables is thus once more two: the ratio Zr/Ti can be expressed by the fraction $x/(1-x)$ and the ratio Ca/Ba by the fraction $y/1-y)$. If $x$ and $y$ are plotted as perpendicular coordinates, then all possible compositions can be found within the square $0<x<1$, $0<y<1$. The position of the ε-peak is mainly determined by the ratio Zr/Ti, thus by the parameter $x$. *Fig. 7* shows the segregation area with the connodes and *fig. 8* the ε-$T$ curves for the four specimens whose compositions are defined in fig 7.

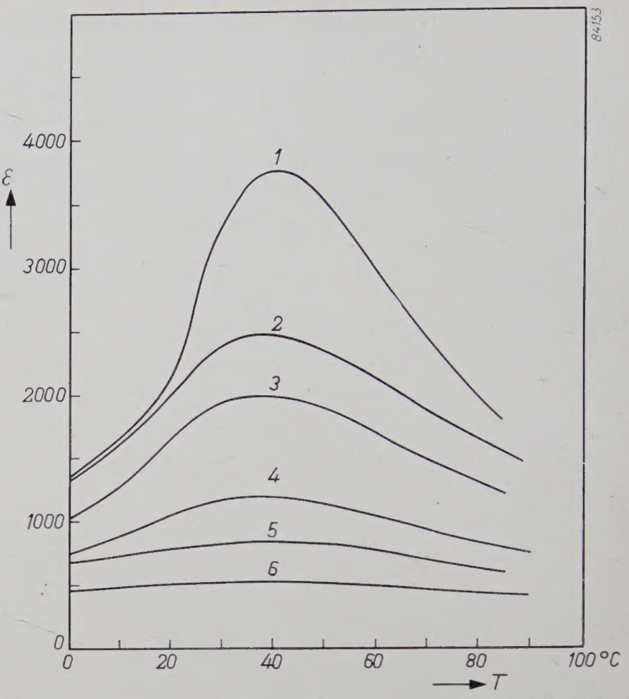

Fig. 6. ε-$T$ curves for sintered specimens, composed of $BaTiO_3$, $SrTiO_3$ and $CaTiO_3$, corresponding to the compositions *1* to *6* in fig. 5. Compositions *3* to *6* lie in the two-phase region and in this order contain increasing amounts of the phase rich in $CaTiO_3$, which makes the ε-$T$ curves increasingly flat.

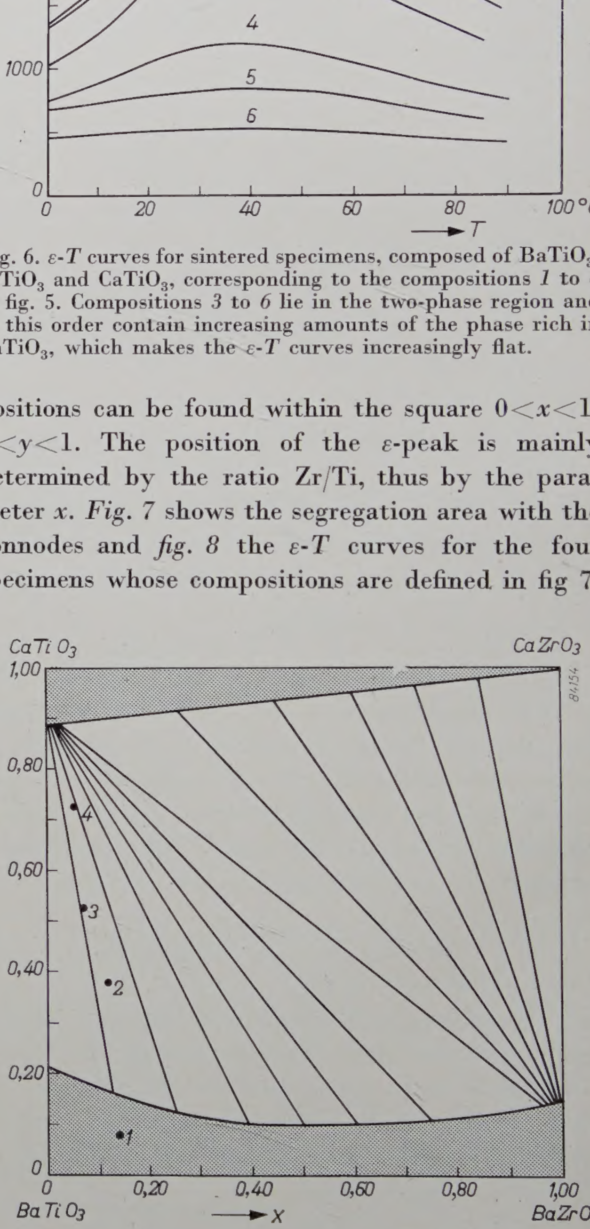

Fig. 7. Phase diagram at 1300 °C of the system $BaTiO_3$-$CaTiO_3$-$CaZrO_3$-$BaZrO_3$ with two perovskite phases (shaded areas). The ratio Zr/Ti is $x/(1-x)$, the ratio Ca/Ba is $y/(1-y)$. The straight lines in the segregation region are the connodes. From the direction of the connodes it can be seen that the combination $BaZrO_3$ + $CaTiO_3$ is more stable than the combination $BaTiO_3$ + $CaZrO_3$.

This system has also been described by Mc Quarrie and Behnke [11]). Our results differ somewhat from their's, especially in the area in the neighbourhood of the $BaTiO_3$ corner, which is so important for practical dielectrics and which we therefore studied more particularly.

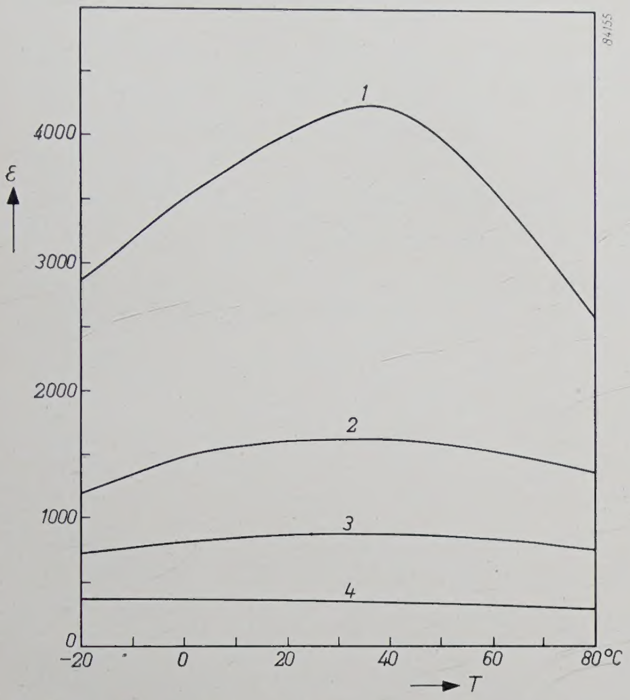

Fig. 8. $\varepsilon$-$T$ curves for sintered specimens prepared from $BaCO_3$, $CaCO_3$, $TiO_2$ and $ZrO_2$, corresponding to the compositions *1* to *4* in fig. 7. Here too, the strong flattening action of the increasing proportions of the phase rich in $CaTiO_3$ is demonstrated.

As was evident from the work of the above-mentioned authors and can be seen from fig. 7, the connodes lie in such a way that the system practically falls into two ternary systems, viz. the systems $CaTiO_3$-$BaTiO_3$-$BaZrO_3$ and $CaTiO_3$-$CaZrO_3$-$BaZrO_3$.

The behaviour expressed in fig. 7 can be more easily understood if the system (Ba, Ca) (Ti, Zr)$O_3$ is compared with a simpler system which behaves in very much the same way, viz. that of Fe-Ni-FeO-NiO. This system is also determined by two parameters, viz. the ratio Ni/Fe and the ratio oxide/metal. For the sake of simplicity, one can assume that no metal dissolves in the oxide and no oxide in the metal. The one-phase areas thus shrink to the sides Fe-Ni ($y=0$) and FeO-NiO ($y = 1$) (see *fig. 9*). If a mixture of Fe and Ni is partially oxidized, mainly FeO will be formed because of the greater affinity of Fe for O. The two-phase lines (connodes) thus become straight lines running from the FeO corner ($x \approx 0$, $y = 1$) to points on the FeNi line ($y = 0$). On the other hand, if a mixed oxide crystal (Fe,Ni)O is partially reduced, mainly Ni will be formed and thus the metal in the diagram is represented by a point which coincides nearly with the Ni corner ($y = 0$, $x \approx 1$). The rest of the diagram is filled with lines joining the Ni corner to points on the NiO,FeO line ($y = 1$). If we turn our attention to the centre of the square ($x = y = 0.5$), we see that for this net composition, the system separates out almost entirely into FeO + Ni and not into the combination NiO + Fe, which corresponds to the other diagonal. This is related to the fact that the reaction NiO + Fe $\leftrightarrows$ FeO + Ni + $Q$ has a positive heat of reaction $Q$ i.e. it is exothermic. The heat of reaction mainly determines the difference in Gibbs free energy because the differences in entropy in this case can be neglected, and this makes the Gibbs free energy of FeO + Ni smaller than that of NiO + Fe, so that the former is more stable.

In the same way the diagonal in fig. 7, running approximately from $CaTiO_3$ to $BaZrO_3$ and dividing the two "ternary" systems, indicates that the reaction

$$BaTiO_3 + CaZrO_3 \leftrightarrows CaTiO_3 + BaZrO_3 + Q$$

is exothermic ($Q > 0$), so that the right-hand combination is the more stable.

A similar behaviour to that described above for (Ba,Ca) (Ti,Zr)$O_3$ is found for the system (Ba,Ca) (Ti,Sn)$O_3$.

If one tries to prepare substances with the composition (Ba,Ca) (Ti,Ce)$O_3$, a two-phase (even partially three-phase) system arises, in which the phase consisting chiefly of $CaCeO_3$ has a small Gibbs free energy. This is to be seen in *fig. 10*, where the diagonal which divides the two nearly ternary systems, now runs from $BaTiO_3$ to $CaCeO_3$, in contrast to fig. 7.

In fig. 10 the substance $CaCeO_3$ is given as $CaO.CeO_2$. The replacement of the Ti-ion by another random tetravalent ion does not, in fact, always lead to compounds of the perovskite type. If one attempts

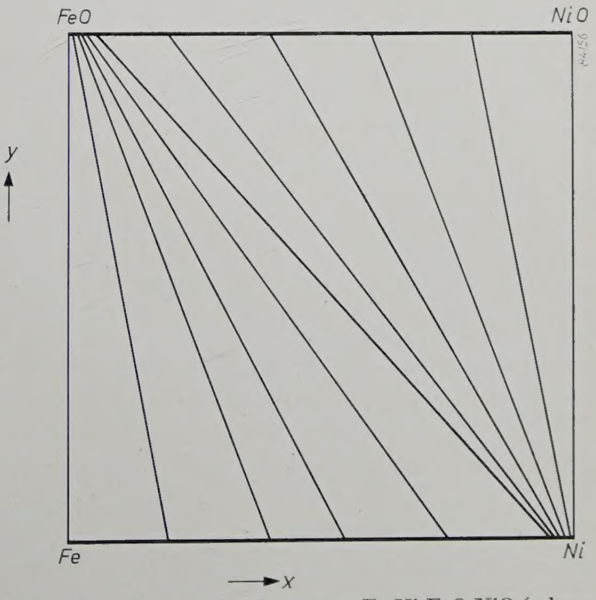

Fig. 9. Phase diagram for the system Fe-Ni-FeO-NiO (schematic). This diagram serves to elucidate fig. 7. The connodes have been drawn in order to demonstrate that the combination Ni + FeO is more stable than the combination Fe + NiO.

---

[11] M. McQuarrie and F. W. Behnke, J. Amer Ceram. Soc. **37**, 539-543, 1954.

to prepare $CaCeO_3$, it appears that this does not crystallize in the perovskite structure, but produces a solution of CaO in $CeO_2$, which, like $CeO_2$ itself, shows the same structure as fluorite [12]). Furthermore, the cerates, including $CaO.CeO_2$, have a fairly small value of $\varepsilon$ ($\varepsilon \approx 35$). Thus the addition of Ce to a (Ba,Ca) titanate has a less favourable result than that of Zr or Sn.

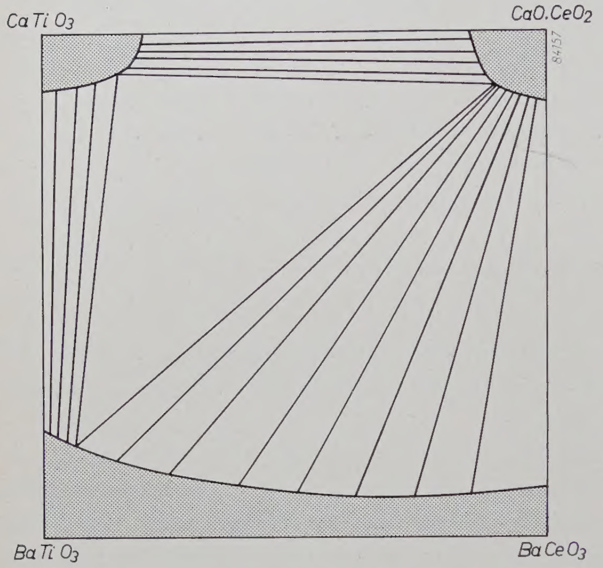

Fig. 10. Phase diagram for the system $BaTiO_3$-$CaTiO_3$-$CaO.CeO_2$-$BaCeO_3$ (schematic). In this diagram, besides the two perovskite phases, a third phase with fluorite structure, occurs in the $CaO.CeO_2$ corner. The Gibbs free energy is so small there that the disposition of the connodes in this diagram differs from that in fig. 7.

## The stability of materials with perovskite structure

The above considerations bring us to the question of the stability of perovskite compounds. The value of the Gibbs free energy (which determines the stability) can be related to the degree to which the ions do or do not fit into the perovskite lattice.

The most important contribution to the Gibbs free energy is, in fact, made by the electrostatic component of the lattice energy (Coulomb energy). If, however, one compares these contributions for the combination $BaTiO_3 + CaZrO_3$ with those for the combination $CaTiO_3 + BaZrO_3$, it appears that when calculated for perfect perovskite structure, they are almost equal. The chief contribution te the lattice energy is $A/a$, where $A$ is the Madelung constant and $a$ the cell dimension for a given component. For the above substances $a$ has the values 4.00, 4.00, 3.92 and 4.18 Å respectively and we find for the first-mentioned combination

$$\frac{1}{4.00} + \frac{1}{4.00} = 0.500,$$

and for the second combination,

$$\frac{1}{3.82} + \frac{1}{4.18} = 0.501.$$

Under these circumstances, secondary influences, such as the fit of the ions in the lattice, become of importance in determining the difference in Gibbs free energy.

A measure of the fit of the ions in the lattice is Goldschmidt's tolerance factor $t$ (see I):

$$t = \frac{R_A + R_O}{(R_B + R_O)\sqrt{2}}. \quad \ldots\ldots \quad (11)$$

Here $R_A$, $R_B$ and $R_O$ represent the radii of the large metal ions (A), small metal ions (B) and oxygen ions (O), all imagined to be spherical. Compositions which fit well, like $SrTiO_3$, have a value $t \approx 1$. Ba compounds also fit fairly well. Ca compounds show greater deviations, as can be seen from *Table II.*

**Table II.** Tolerance factor t for various perovskite compounds, calculated with the help of ion radii corrected according to Zachariasen.

| | | | |
|---|---|---|---|
| $CaTiO_3$ | 0.94 | $BaTiO_3$ | 1.07 |
| $CaSnO_3$ | 0.91 | $BaSnO_3$ | 1.025 |
| $CaZrO_3$ | 0.87 | $BaZrO_3$ | 0.98 |
| "$CaCeO_3$" | 0.82 | $BaCeO_3$ | 0.92 |

If one takes the value of $|t - 1|$ as a measure of the Gibbs free energy, then the most stable combination in the (Ba, Ca) (Ti, Zr)$O_3$ system will be found to be $BaZrO_3 + CaTiO_3$. In the (Ba,Ca) (Ti, Ce)$O_3$ system discussed above, the combination $BaCeO_3 + CaTiO_3$ would be the more stable according to the table. But the "compound" $CaO.CeO_2$ which, as stated above, possesses a fluorite structure, has a so much smaller Gibbs free energy than the hypothetical $CaCeO_3$ that as a result the other combination, $BaTiO_3 + CaO.CeO_2$, is the more stable.

## Effect of foreign admixtures

Up to now we have spoken mainly about influencing the behaviour of $BaTiO_3$ by formation of mixed crystals with substances which also have a perovskite structure. It has also become apparent that many other substances will dissolve in small quantities in $BaTiO_3$ and sometimes have a marked effect on the form of the $\varepsilon - T$ curve. It is not yet known with certainty whether their influence is due to their hinderance of the crystal growth or to some specific influence in the material itself. In either case, the transition temperatures are not shifted (or are shifted only very slightly); the added quantities are too small for that. Probably the principal action is upon the crystal growth during the sintering process and in hindering the transition from the cubic to the tetragonal phases. This change in crystal structure occurs by a whole row of ions of one kind moving with respect to a row of another kind. If the crystal structure is now disturbed by

---

12) H. Gränicher, Helv. Phys. Acta **24**, 619-622, 1951.

solutions of foreign materials which do not fit into the perovskite structure, the change can be wholly or partially hindered. A favourable additional effect is that foreign admixtures cause the dielectric hysteresis loop to be considerably flattened, so that the non-linear properties which pure $BaTiO_3$ exhibits strongly below 123 °C partly disappear.

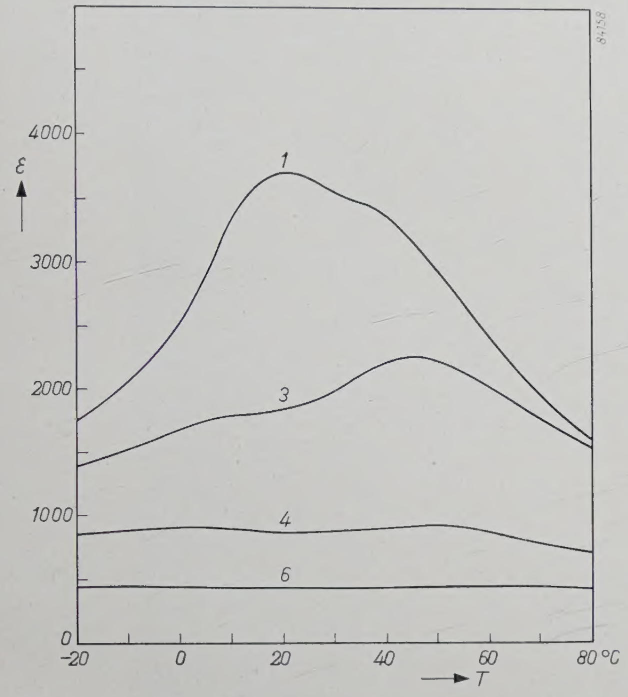

Fig. 11. $\varepsilon$-$T$ curves for a series of specimens in the $BaTiO_3$-$SrTiO_3$-$CaTiO_3$ system to which about 10% $Mg_2TiO_4$ has been added. The compositions (calculated without the $Mg_2TiO_4$) of 1,3,4 and 6 correspond approximately with the similarly numbered points in fig. 5. The effect of the additive is to make the curves flatter than those in fig. 6.

An objection, however, is that some impurities only temporarily hinder the crystallographic transition, i.e. they only slow it down. This results in prolonged after-effects, which are observed as a prolonged continuous decrease in the dielectric constant in material which has been cooled from a temperature above the transition point to room temperature.

One substance which has been successfully used to improve the $\varepsilon$-$T$ curve is magnesium oxide, which is added to the (Ba,Sr,Ca)$TiO_3$ system in the form of $Mg_2TiO_4$. Some $\varepsilon$-$T$ curves for these specimens are shown in *fig. 11.*

The work discussed here has been carried on in co-operation with V.I. Middel of the Material Research Laboratory, Philips Electrical Ltd, Mitcham (England), J. Möllers of the Deutsche Philips Ges.m.b.H. Keramische Werke, Hamburg and G. H. Weber and N. W. Smit of the Ceramics Laboratory at Eindhoven.

**Summary.** $BaTiO_3$ and related compounds of the perovskite structure show very high values of the dielectric constant. In certain temperature ranges, $\varepsilon$ shows peaks corresponding to crystallographic transition points. Since the values of the transition temperatures are sensitive to all kinds of influences (internal stresses, surface phenomena, lattice imperfections) the manner in which the material is fired has a great effect upon the shape of the $\varepsilon$-$T$ curve. This curve can be further influenced by the formation of mixed crystals (displacement of the peaks), by diluting the material with a second phase which has a flatter $\varepsilon$-$T$ curve, and also by the addition of small quantities of foreign substances (such as $Mg_2TiO_4$) which do not crystallize themselves in perovskite structure but still manage to enter the material either as a solution or between the crystals. Such admixtures help, at the same time, to suppress the dielectric hysteresis.

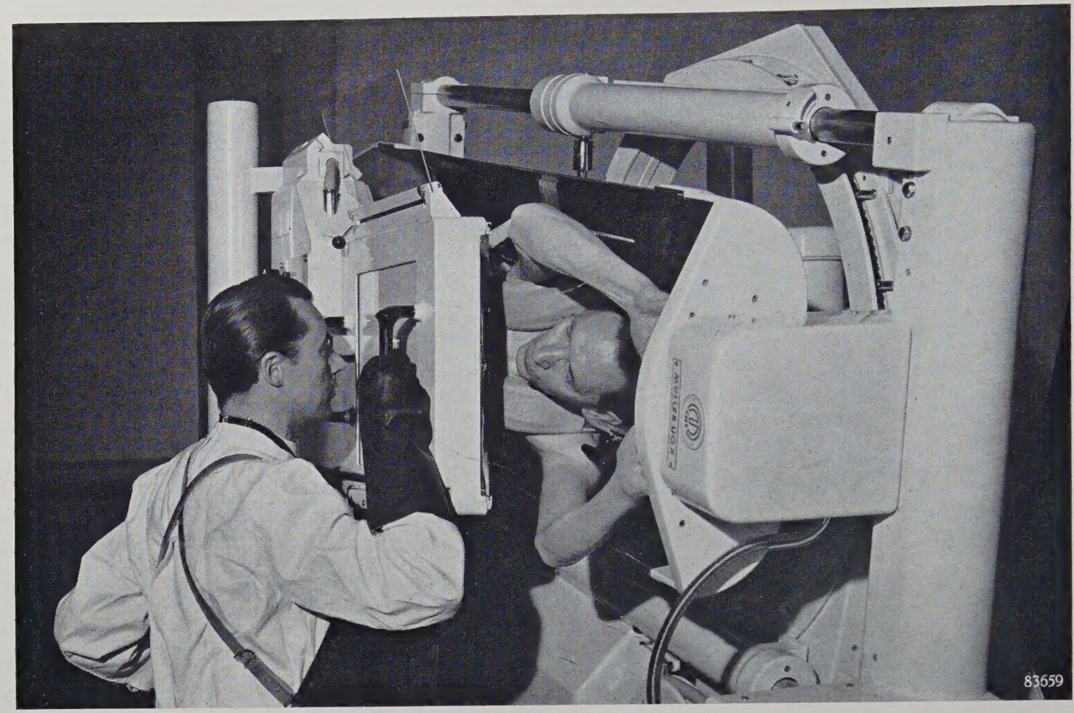

# A NOVEL TYPE OF DIAGNOSTIC X-RAY UNIT

by H. VERSE *) and K. WEIGEL *).

616-073.755.1

*In general, the designers of practical medical equipment must be guided by medical opinion. This applies particularly to X-ray diagnostic apparatus, whose special feature is an effective combination of mechanical, electrical and optical components. The apparatus described in the present article is novel in that, to improve the above-mentioned combination, the designers have ventured to suggest to the radiologist an examination procedure which is in some respects new and should be complementary to the older and more familiar methods of examination.*

## Principles of the apparatus

The problem of mechanical aids for medical X-ray examination was discussed in a recent issue of this Review, in connection with a description of the "Symmetrix" [1]). The "Symmetrix" belongs to a class of apparatus now employed for routine diagnostic examinations in almost all countries. The essential feature of such apparatus is that it enables the examination table to be rotated about a horizontal axis at right angles to the X-ray beam, from the vertical to the horizontal position and beyond it (Trendelenburg position); with the most advanced equipment of this type, say, the "Symmetrix", the table can be rotated even far enough to invert the subject. As the table carrying the patient tilts, the X-ray tube and the viewing system (fluorescent screen and serial cassette) move with it. Moreover, the X-ray tube and viewing system can be moved, within certain limits, parallel to the table and the viewing system can be shifted at right angles to the table surface. The balancing of the movable parts of the "Symmetrix" is described in the article referred to in note [1]).

The "Symmetrix" is a development on conventional lines, based on examination procedures to which radiologists are already fully accustomed. The diagnostic unit to be described here, however, is based on quite different ideas. In this apparatus (type UGX) designed in Hamburg, the X-ray beam remains horizontal and at eye-level (*fig. 1*) [2]). The patient is strapped in a special cradle (which is transparent to X-rays) situated between the X-ray tube and the fluorescent screen. This cradle, driven by motors and controlled from the position of the radiologist, enables the subject to be shifted and rotated so as to position the required part of the body in the X-ray beam at an angle corresponding to the desired projection [3]), enabling different positions of the internal organs relative to the direction of gravity to be obtained.

---

*) C. H. F. Müller Aktiengesellschaft, Hamburg.

[1]) J. J. C. Hardenberg and H. W. Dumbrill, The "Symmetrix", a universal table and stand for X-ray diagnosis, Philips tech. Rev. **17**, 112-120, 1955/56 (No. 4).

[2]) H. Verse and K. Weigel, Eine gerätetechnische Betrachtung zur Röntgendiagnostik, Fortschr. Röntgenstrahlen **80**, 520-524, 1954 (No. 4).

The development of this apparatus is based on the general premise that with the advance of X-ray technique it will become more and more difficult to satisfy the requirements imposed by the conventional examination procedures referred to at the beginning of this article. Viewing systems are becoming more and more complex; for example, there is a tendency towards higher tube voltages, necessitating heavier shields on the screen as protection against scattered radiation; an X-ray image intensifier with its viewing system may be used instead of the ordinary fluorescent screen; again, the viewing system may be provided with special attachments, e.g. a camera mount for miniature radiography or an X-ray image intensifier and ciné camera. Owing to the size and weight of such attachments it is no simple matter to enable them to be moved with the table, and the problem of balancing becomes almost insuperable when the possibility of making them interchangeable is also considered. Moreover, there is the important question of the physical strain imposed on the radiologist during an examination. Despite motors to enable the table to be tilted, and the viewing system and associated counterweights to be shifted, almost without effort, the mere act of following the movements of the fluorescent screen or image intensifier imposes a considerable strain on the radiologist.

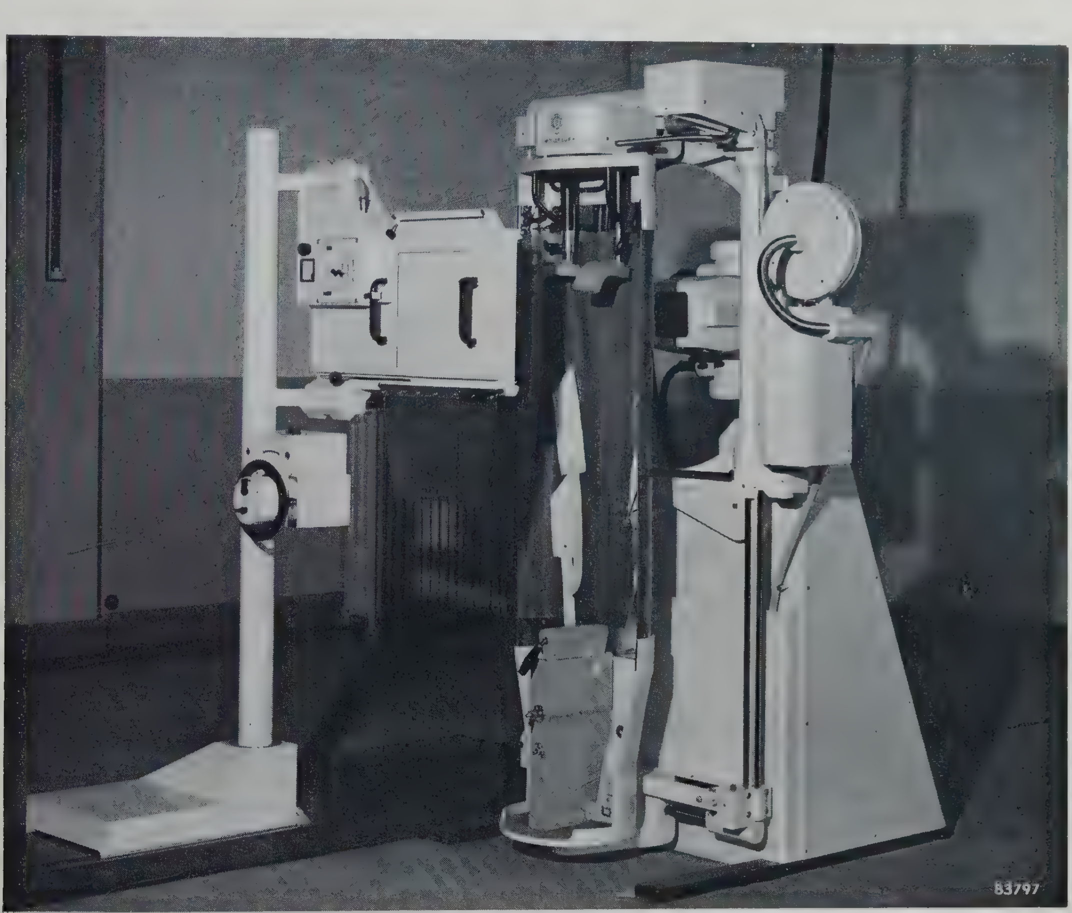

Fig. 1. The "Müller" UGX diagnostic X-ray unit. The column seen on the left of the picture, running on floor rails, carries the viewing system and the control box; a cradle of thin wood, to carry the patient, supported by a frame mounted on the base is seen in the centre of the picture; on the right of the cradle and base is the X-ray tube, on a separate stand, also on floor rails.

None of these objections apply to the new unit shown in fig. 1. It enables the radiologist to carry out any examination whilst standing comfortably erect and looking straight in front of him. The only physical effort involved is that required to move the viewing system horizontally either towards or away

---

[3]) The unit considered here is employed mainly for the examination of organs in the trunk of the patient.

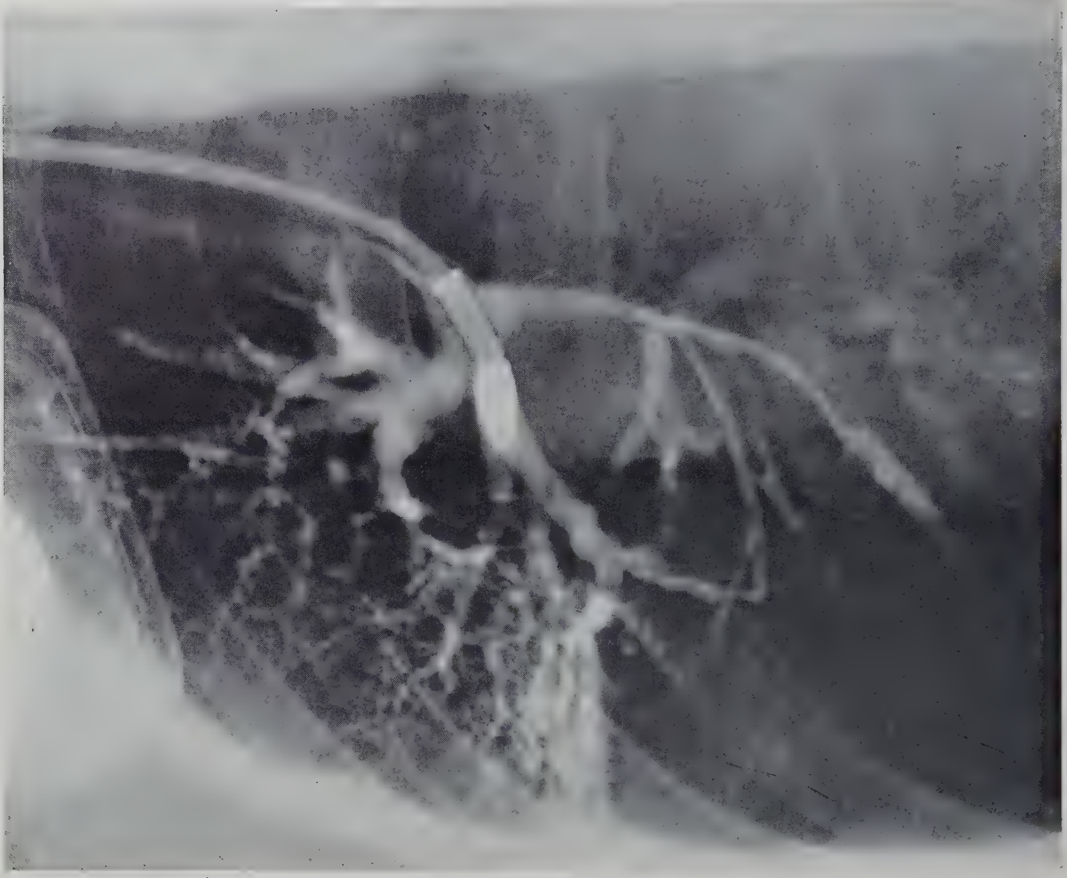

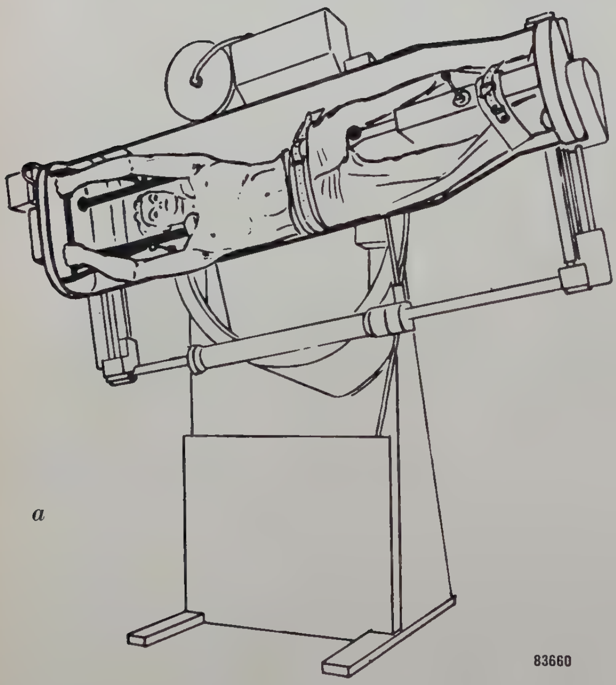

Fig. 2. Example of bronchography with the "Müller" UGX. The subject lies on his right side, tilted slightly with his head downwards (*a*). Contrast medium is injected into the bronchia by means of a cannula. The X-ray picture (*b*) shows the nozzle of the cannula and the branch of the trachea leading to the centre lobe of the right lung. Most of the branches of the top lobe, seen on the left of the picture, are filled with contrast medium, enabling their variations to be readily appraised. The branches of the bottom lobe are only partly filled.

from the patient, a movement which needs no balancing against the force of gravity. Moreover, apparatus so designed eliminates the above-mentioned problems associated with the interchanging of the different attachments for viewing and recording the X-ray image. Also, the radiologist can be given very much better protection against scattered radiation, with less discomfort to himself, because this apparatus is operated almost from one position. On conventional equipment the radiologist must move about for the examination of the patient in various positions and is obliged to carry a considerable weight of lead on his person in order to be roughly equally protected in all positions.

Considering the diagnostic possibilities of the new unit, it will be noted that the possibility of tilting the patient together with the X-ray beam in the conventional manner has been deliberately abandoned. Accordingly, this apparatus cannot be employed instead of the existing equipment to diagnose cases for which the above-mentioned method of examination is indispensable. On the other hand, it gives scope for a considerable extension of the existing possibilities through a series of entirely new patient-positions and projections. Experience b

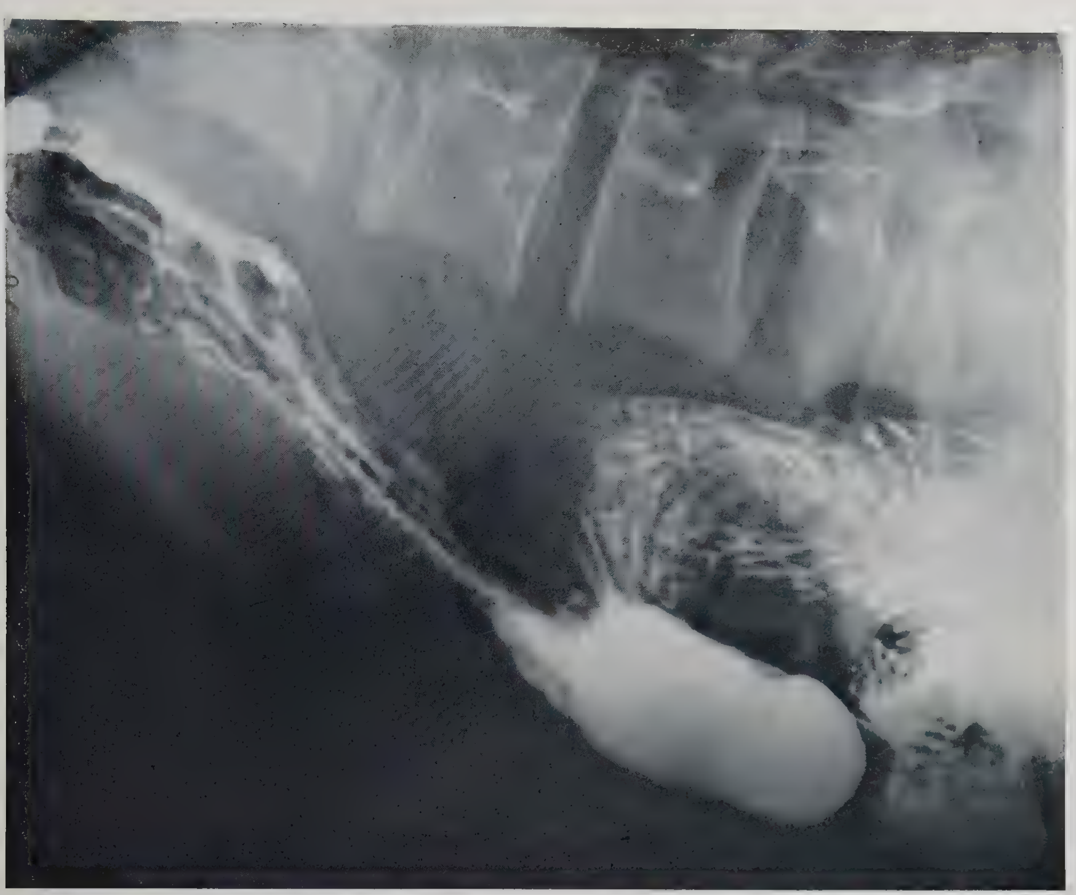

a

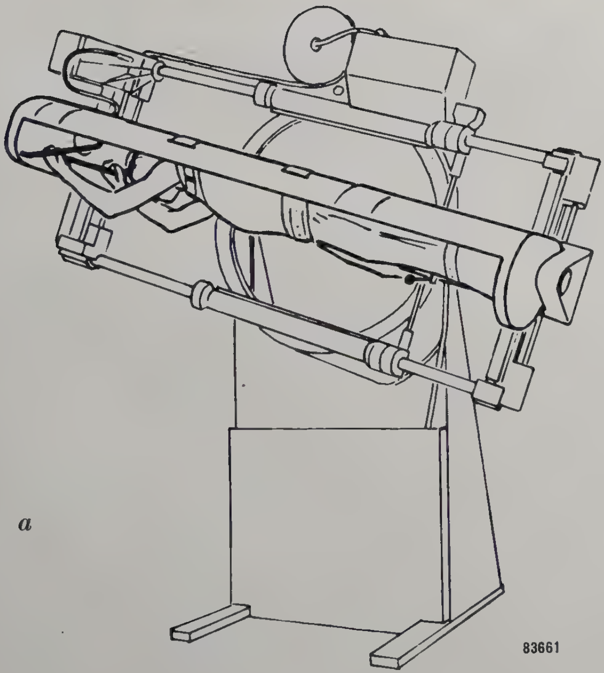

Fig. 3. Example of stomach radiography with the "Müller" UGX. The subject is virtually prone, but tilted feet downwards at roughly 20° (*a*). This novel position gives an unusually clear view of the front and rear walls of the stomach and of the position of the duodenum. The entrance to the stomach, with the air bubble, always present in the stomach, rising into it, is seen at the top left-hand corner of the radiograph (*b*). Stretching diagonally across the picture towards the bottom right-hand corner is the long middle tract of the stomach. The contrast medium has settled in the lower end. The stomach exit is concealed behind the completely filled tract, but the duodenum, joining this exit, is seen freely projected between the filled tract and the spinal column.

with the apparatus so far has shown that these new facilities may well constitute a very useful adjunct to the conventional examination procedures. Two of the new patient-positions, together with the associated X-ray pictures, are shown in *figures 2* and *3*.

Another point worth mentioning is that the apparatus provides many of the practical facilities of so-called universal X-ray diagnostic units. For example, it can be adjusted for taking pictures at a distance, or to project an enlarged shadow picture, merely by moving the X-ray tube or viewing system horizontally. Similarly, in stomach examinations, a precisely regulated compression of the subject can be effected (see for example [1])). The apparatus is also suitable for planigraphy, as will be explained later.

## Design of the unit

The essential feature of the new unit is the cradle and drive, enabling the radiologist to move the subject in the directions indicated by arrows in *fig. 4*. The design of the cradle and drive may now be explained with the aid of *fig. 5*. The principal components are the cradle itself, in which the patient is placed (or laid), a frame to carry the cradle and enable it to be rotated and translated, and a sturdy, bottom-heavy base carrying a large ring ball-bearing. This bearing — in principle of the same type as conventional ball bearings — comprises two rings, one fixed to the base and the other, driven by an electric motor (in the base) carrying two cylindrical slides for the longitudinal tubes of the frame. The latter, which carries the cradle, can thus be moved across the bearing. This enables the patient to be moved up to 90 cm longitudinally. Power for this movement is supplied by an electric motor, mounted on the rotating ring of the large bearing and geared through an intermediate spindle to two pinions in the end pieces of the cylindrical slides; these pinions engage with racks along the backs of the long tubes of the frame.

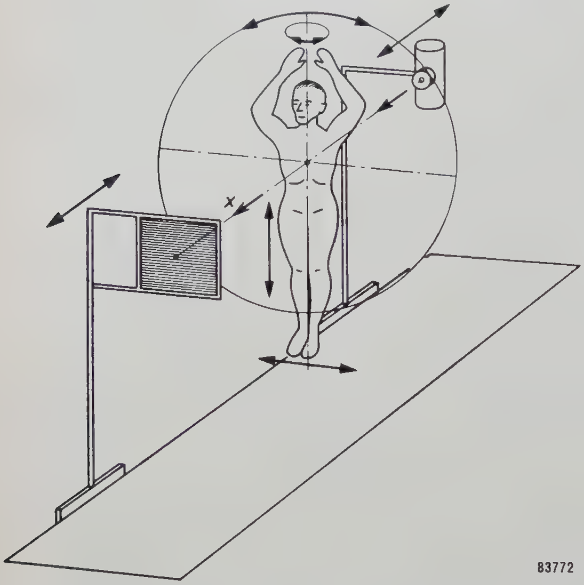

Fig. 4. Degrees of freedom of the patient, the X-ray tube and the viewing system in the "Müller" UGX diagnostic unit. The centre-line of the X-ray beam remains in a fixed horizontal position throughout these movements.

The lateral tubes at the top and bottom of the frame carry rails for head and foot members with bearings to support the cradle. Inside these tubes are threaded spindles, coupled together by a spindle in one of the long tubes and driven by an electric motor attached to the lateral tube at the head of the frame. These spindles engage with threaded bushes on the head and foot members of the cradle, thus driving them at the same speed along the rails. In this way, the patient can be moved 18 cm in

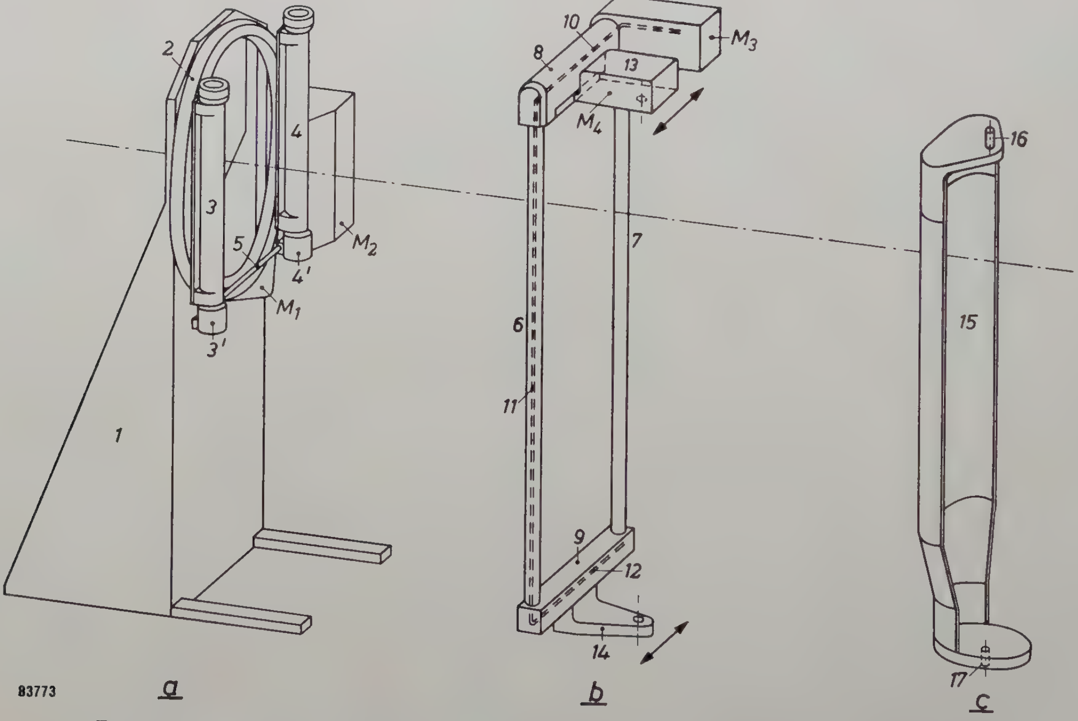

Fig. 5. The various parts of the cradle and drive. *a*) Base *1* of the diagnostic unit, with electric motor $M_1$ to drive the rotating ring of the large ball bearing *2*; cylindrical slides *3* and *4*, and electric motor $M_2$ to drive the pinions in the end-pieces *3′* and *4′*; *5* coupling spindle. *b*) Frame, with long tubes *6* and *7* fitted with racks and supported by slides *3* and *4*; *8* and *9* lateral tubes; $M_3$ electric motor to drive the head and foot members *13* and *14* through spindles *10*, *11* and *12* and thus move the cradle and patient laterally. *c*) Cradle *15*, with short spindles *16* and *17* fitting into bearings in the head and foot members *13* and *14*; spindle *16* is driven by another electric motor ($M_4$, in *b*) to rotate the patient about his longitudinal axis.

either direction at right angles to his longitudinal axis.

Short spindles at both ends of the cradle fit into thrust bearings in the head and foot slides. An electric motor housed in the head slide drives the head spindle through a reduction gear to rotate the cradle about its longitudinal axis, enabling the patient to be turned a full 360° in either direction. Hand grips and shoulder supports at the head, and a leg support at the foot of the cradle, together with various belts and buckles, hold the patient firmly and give him a feeling of complete safety, even in positions such as those shown in figures 2 and 3.

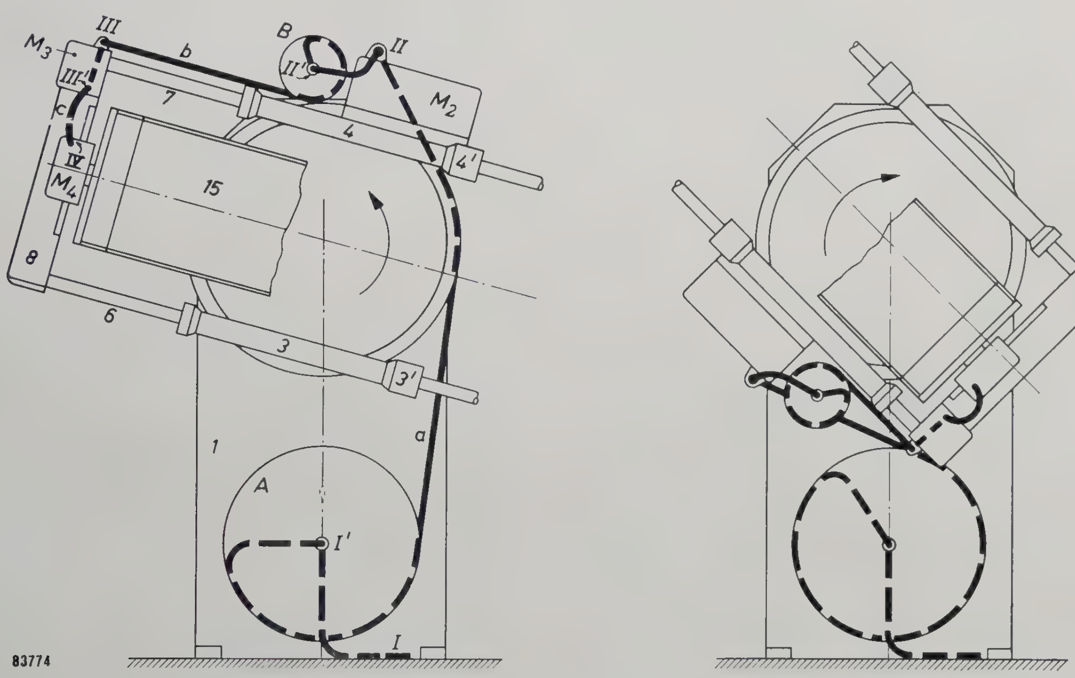

Fig. 6. Connecting cables on the equipment. During all movements, cable sections *a* and *b* are held taut between terminal points *I*, *II* and *III* by spring-loaded cable-drums *A* and *B*. Section *c* is prevented from sagging by a wire spiral fitted round it. Other components numbered as in fig. 5. The diagram on the right shows the change in the configuration of the cable sections when the patient is adjusted to another position.

It is seen that only one of the motors, that is, the one driving the rotary ring of the large bearing, is secured to the base. The motors for the longitudinal and lateral movements, and that to rotate the cradle, are mounted on moving parts of the apparatus. Moreover, most of the limit contacts and change-over switches, employed (see below) to control the different movements, are likewise attached to moving parts. Accordingly, it was necessary to design a special cabling system to connect them. Owing to the number of connections involved it was not practicable to employ slip rings; hence another system, shown in *fig. 6*, was adopted (see also fig. 1); all the leads are enclosed in one, flexible, multi-core cable, running to the furthest terminal on the head slide and held taut, without sagging loops, in every position of the cradle. This cable is divided into three sections (*a*, *b* and *c*). The first section runs from a fixed terminal (*I*) in the base of the apparatus to a point (*II*) near the electric motor on the rotating ring of the large bearing; the second section connects this point to another (*III*) on the lateral tube at the head of the frame, and the third one connects the frame to the head slide of the cradle (*IV*). Since the distance to the head-slide to be covered by the last length of cable (*c*) varies only slightly, it is taken in a simple loop, held taut by a wire spiral fitted round the cable. On the other hand, sections *a* and *b* must span very considerable ranges of movement. The cable slack required for this purpose is taken up by two suitably positioned cable drums (*A* and *B*). Both these sections of cable run from their fixed points (*I* and *II*) to the correspondingd rum, entering through the hollow drum-spindle (*I'* and *II'*). They then cross to a guide on the inner face of the drum and thence span the latter over whatever angle is necessary for the position of the cradle (see fig. 6). Leaving the drum tangentially, they pass to the subsequent fixed points (*II* and *III*). The drums are spring-loaded and so keep the unsupported lengths of cable taut. The cable itself is extra flexible, enabling the cores to move freely in relation to one another and to the cable sheath, and so absorb the torsion occurring at the entries to the drums.

**Control of cradle and drive**

As we have seen, the radiologist controls the cradle from his position near the viewing system. For this purpose, a control box is mounted on the latter, within easy reach of his left hand (fig. 1 and *fig. 7*). On the front of the box is a handwheel to control the rotation of the subject, in either direction, about the axis of the horizontal X-ray beam; in the hub of this wheel are two switches to control the longitudinal and lateral movements of the subject. Another switch, to control the rotation of the subject about his longitudinal axis, is located on top of the control box.

To enable the apparatus to be operated without difficulty in a darkened room, the hub of the handwheel, with the two switches to move the subject longitudinally and laterally, is made to rotate with the subject, that is, in the same direction and with the same angular velocity, by means of a motor housed in the control box. This ensures that the movement of the hand manipulating the control switches produces a corresponding movement of the subject, regardless of how he is tilted (*fig. 8*). All the various movements have limit contacts in suitable positions, which switch off the associated driving motor when the limit of the movement is reached. In this way rotation about the horizontal X-ray beam is limited to 180° clockwise and 180° anti-clockwise; the patient can thus be tilted to the inverted vertical position in either direction.

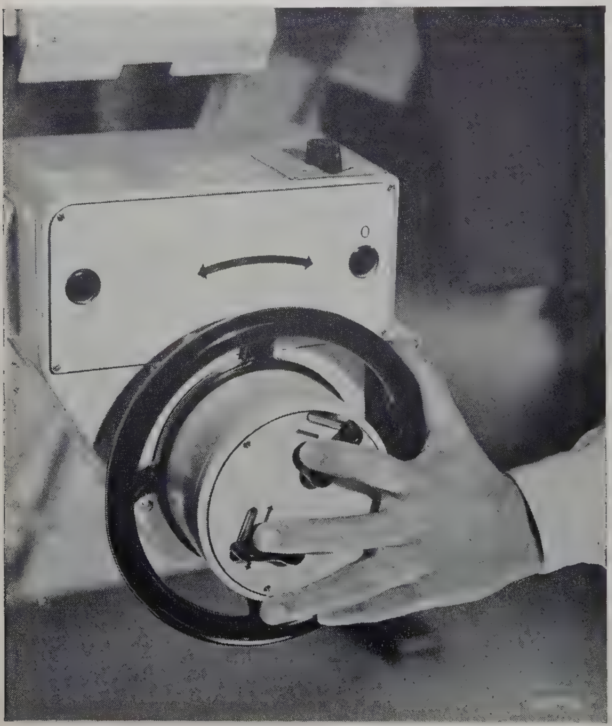

Fig. 7. The control box. The hand wheel controls the rotation of the patient about the horizontal X-ray beam. The two switches on the hub of this wheel control the longitudinal and lateral movements of the patient, and the switch on top of the box controls the rotation of the patient about his longitudinal axis. When the button *0* on the right is pressed, all the moving parts of the apparatus return to their normal positions. The button on the left enables the whole apparatus to be stopped immediately in an emergency.

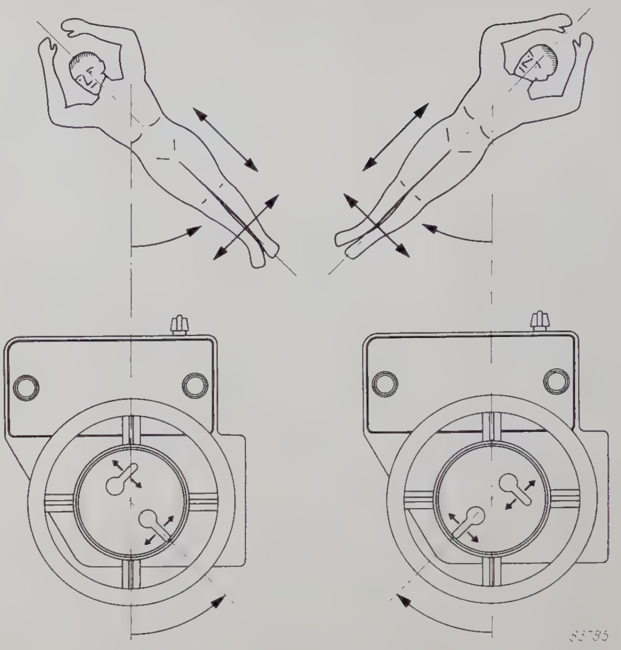

Fig. 8. The hub of the hand wheel driven by a small motor housed in the control box, rotates with the patient so as to maintain the switches in the same positions relative to the patient-movements controlled by them.

To return the subject to the normal position after an examination, the doctor merely presses a button at the front of the control box (*0* in fig. 7). The initial movement of any of the parts of the apparatus away from the normal position, operates one of two toggle switches, according to the direction of the movement. This in turn energizes a relay which ensures that each motor rotates in the proper direction when the return-button is pressed. On reaching their normal positions, the various moving parts operate other limit contacts which switch of the driving motors automatically. The rotating part of the control box, carrying the two switches, is similarly controlled. The cradle and the rotating hub of the control box thus return to the same relative positions after each examination; hence, although the motors are asynchronous, cradle and hub can never be out of phase with each other, since any slight variations that may occur are not cumulative.

The relay system for the operation of these controls is housed in the base of the apparatus (*fig. 9*).

### Planigraphy

There may be some doubt as to why it is necessary for the main bearing to have so large an inner diameter, since in principle the X-ray beam would have plenty of room to pass through a very much smaller one. However, this large bearing was chosen to make possible the use of one or two accessories which enable the apparatus to be employed for planigraphy. This secondary function involves swinging the X-ray beam, fixed for all other purposes, through a given angle about a particular point in the body of the patient. *Fig. 10* shows a model demonstrating how this may be done. In the model the X-ray tube is swung in such a way that the central ray of its beam remains in the vertical plane of symmetry of the apparatus. The film cassette must move with the central ray in planigraphic exposures; hence the viewing system is shifted away from the normal operating position to make room for a column carrying a movable film cassette (and if necessary, a Potter-Bucky diaphragm).

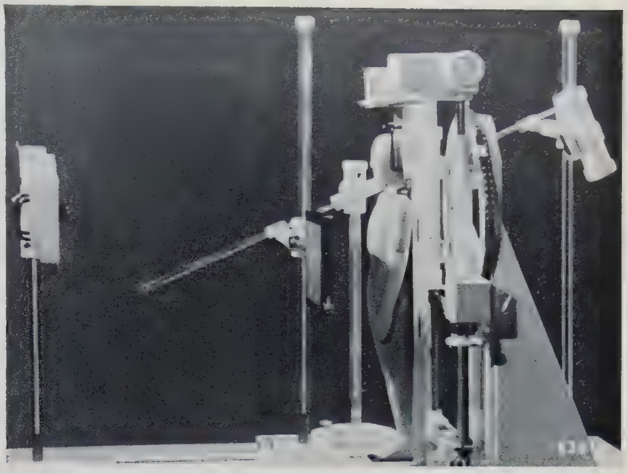

Fig. 10. Model of the UGX diagnostic unit as set-up for planigraphy. The fluorescent screen is not required; it is moved away to make room for a film cassette mounted on a separate stand and connected to the X-ray tube by a coupling rod.

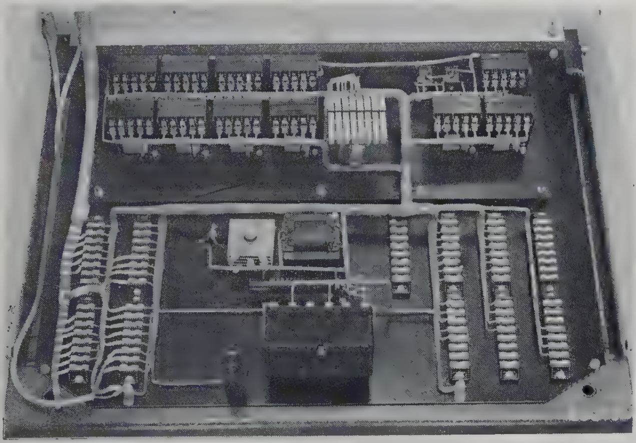

Fig. 9. Relay system, housed in the base of the apparatus, through which the limit contacts, "memory" switches, etc., control the various movements.

**Summary.** One of the characteristic examination procedures carried out with so-called universal X-ray diagnostic equipments consists in tilting the patient, together with the X-ray tube and the viewing system, about a horizontal axis at right angles to the X-ray beam. With the "Müller" UGX diagnostic unit, however, this procedure, and in particular the associated vertical examination of patients in the horizontal position, is dispensed with. The X-ray beam of this new apparatus remains in a fixed horizontal position. A movable cradle between the X-ray tube and the fluorescent screen enables the patient to be rotated about an axis coinciding with the horizontal X-ray beam; moreover, the patient can be moved longitudinally and laterally, and rotated about his longitudinal axis. The radiologist, standing in front of the viewing system, controls all the motor-driven parts of the apparatus with the aid of a conveniently placed control box. The principal advantage of this arrangement is that it facilitates the use of modern diagnostic aids such as the X-ray image intensifier and the ciné camera in examinations, and minimizes the physical strain on the radiologist, even when using very hard X-rays which require heavy protective screening. Instead of the conventional examination procedure dispensed with, the apparatus permits several entirely new patient positions and unusual projections, one or two examples of which are given.

# RESEARCH ON THE CONTROL OF ANIMAL PESTS

by J. MELTZER *).

632.9:632.6/.7

*Agriculture and horticulture must conduct a perpetual battle against plant diseases and pests. The dangers that threaten when adequate quantities of pest control agents are not kept at hand, were brought home only last year by the locust plague in Morocco, where in a short space of time enormous damage was inflicted. At Boekesteyn *) and elsewhere an intensive search is in progress to extend the arsenal of chemical combating agents. Research at Boekesteyn has led, inter alia, to a new agent for combating the spider mite.*

Cultivated plants are continuously exposed to attack, and even to destruction, by various diseases and pests. A review of such injurious influences, together with the chemical means at our disposal for combating them appeared recently in this journal $^{1}$). As explained in that article (hereafter referred to as I), pests can be divided into two types: vegetable (fungi, weeds) and animal. We shall be concerned here only with the latter class.

Although the animal kingdom embraces the most divergent creatures, from the primitive microscopic, non-cellular, animalcules (Protozoa) to the largest mammals, the insects form far and away the greatest class. According to Imms $^{2}$), 70% of all the known species of animals belong to the insects, i.e. 700 000 species, while it is conjectured that this is less than a fifth part of the number of species of insects which actually exists. In this group is found the majority of injurious animals. It should not go unmentioned that there are also many useful insects, useful either because they bring about fertilization of plants, or because they are the natural enemies of injurious animals. The existence side by side of harmful and useful insects renders the control of the former a complex problem.

After the insects, the most important harmful animals are the rodents (rats, mice), snails, worms (especially certain eelworms) and the mites, related to the insects, which belong to the spider family (*Arachnida*). At Boekesteyn various species of experimental animals are cultured on a large scale, including flies (see fig. 2 of article I), grain-weevils, flour-moths, flour beetles (*Tribolium*), colorado beetles, thrips (*Thysanoptera*), spider mites, etc.

## Stomach poisons and contact poisons

Before going into the work carried out at Boekesteyn, it will perhaps be profitable to dwell for a moment on the historical development of insecticides, for this will give us at the same time an idea of the action of these substances.

According to its mode of action, a poison is known either as a stomach poison or a contact poison. In the last century only general (as opposed to specific) stomach poisons were available for combating insects, e.g. lead arsenate. These poisons, however, were not only active against insects, they were also dangerous to all animals and to man. Another disadvantage of stomach poisons is that they are only lethal to insects if the latter eat a relatively large amount of leaf. Sucking insects and spider mites on the other hand, which do not eat the leaves, but pierce their proboscis into the plant to take up the plant juices, are not killed by a stomach poison which covers the surface of the plant. In combating these pests, use must be made of a contact poison.

### *Mineral and vegetable contact poisons*

At the end of the 19th century, paraffin and tar oil came into use as contact poisons against scale insects (*Coccidea*). Later, special mineral and tar oils were developed for combating the winter eggs of various insects and spider mites, which pass the winter at the egg stage on fruit trees.

We cannot here go into the mode of action of these oils. It is sufficient for our discussion to know that they function not as stomach poisons but as contact poisons. Their applicability, however, is seriously limited by the fact that they can only be used when the trees are bare of leaves, since otherwise they would do more harm than good.

The first contact poison that was used against insects was of vegetable origin: nicotine, which at the end of the 17th century was applied on a small scale in the form of tobacco juice. But this poison, too, is extremely dangerous to man and is rapidly absorbed through the human skin. When, around 1925, ground Derris root came onto the market, it was a great advance, for this product was shown to contain a contact poison (rotenone) which, although very strongly active against insects, is but slightly toxic to man. It was, moreover, far cheaper than nicotine and the pyrethrins (prepared from *Pyrethrum*) which had been discovered in the meantime and which are still used in the home against insects.

---

*) Agrobiological laboratory Boekesteyn, N.V. Philips-Roxane, 's-Graveland (Holland).

[1]) R. van der Veen, "Boekesteyn", the agrobiological laboratory of N.V. Philips-Roxane, Philips tech. Rev. **16**, 353-359, 1954/55 No. 12).

[2]) A. D. Imms, A general textbook of entomology, Methuen, London 1946.

### *Synthetic organic contact poisons*

With the discovery of DDT [6] [3]), the first synthetic organic contact insecticide came onto the market. It would take us too far from our subject to describe the revolutionary consequences which this has had for the combating of insects. Sufficient be it to say that this discovery gave the chemical industry the great stimulus to explore this field further.

One of the reasons for this was mentioned briefly in article I: caution must be exercised to ensure that the natural enemies of the insect species to be exterminated are not destroyed. The ideal would require the availability of a number of compounds, each of which was active against one harmful insect species, without being poisonous to other animals — a series, that is, of highly specific (selective) compounds.

Another reason for the intensive research is the noteworthy fact that, however effective an insecticide may be against a few or even a large number of pests, there are always some insect species which in some way or another escape the lethal action. It will suffice to mention only one of the causes: many insect species are naturally protected by their structure, mode of life, or physiology against the action of certain poisons. Some for example live *within* the plant (in wood, bark, leaf or stem) and by reason of this are difficultly accessible from without; such pests can only be combated from within the plant.

### Emphytic (systemic) agents

All the above mentioned insecticides are either sprayed or dusted onto the plant. They might therefore be called *ectophytic*, i.e. *outside* the plant. An ectophytic contact poison kills both friend and foe among insects, for neither parasites nor predatory enemies of the insect to be exterminated nor even bees are spared. Another drawback with ectophytic insecticides is that the shoots which the plant puts forward after treatment, do not share in the protection. Moreover, the applied layer is exposed to sun, rain and wind, so that under unfavourable weather conditions it may rapidly lose activity.

These disadvantages do not hold, or hold to a lesser degree, for poisons which are taken up *into* the plant and are dispersed throughout the whole plant in the sap streams. Young shoots which are put out after the treatment are protected from the very beginning; the weather no longer has a direct influence; insects living in the plant, of which something was said in the previous section, come within the reach of the poison, as well as sucking insects and mites, while useful insects which neither feed on parts of the plant nor suck up its juices, run no danger.

Combating agents which are assimilated by the plant are now often called systemic insecticides. Following Prof. Kuenen we prefer to replace the less accurate term systemic by *emphytic*, a term which implies both *in* and *throughout* the plant and forms a clear antonym to ectophytic. The emphytic agents so far known, for example schradan [12], are all very toxic to man (which is likewise one reason why the ectophytic agents, in spite of the disadvantages summarized, have by no means seen their day).

### Artificial resistance

This survey would be incomplete without some mention of artificial resistance, i.e. a resistance which is built-up in certain insects by some insecticides. Thus, flies are known which have become resistant to DDT, and there are mites which have even acquired resistance to highly poisonous parathion [10].

Due account must be taken during research of the possibility that resistance may be set up. At Boekesteyn resistant flies are regularly included in the investigations, as we shall see presently.

### Research at Boekesteyn

From the foregoing it will hardly be surprising that in the search for means of controlling animal pests our interest is mainly in the field of contact poisons; a stomach poison is only of real interest when it appears to have an emphytic mode of action. A further line of investigation is dictated by the need for specific agents, which do not attack the enemies of the insect to be exterminated, are only mildly toxic to man and domestic animals and evoke no, or only a very slight degree of resistance.

---

[3]) The numbers in square brackets refer to the structural formulae in the appendix.

In addition it is required that a spray or dust residue on the plant is able to kill insects alighting upon it. Use is only very seldom made of methods in which the insects themselves are dusted or sprayed.

Part of the research at Boekesteyn is carried out "under glass" and part on the living plants. This is followed — as was outlined in article I — by a continued investigation of those compounds which have passed the primary test.

### Investigations under glass

For testing the action of compounds against grain-weevils and flies, petri dishes are employed, covered on the inside with a coating of the compound under investigation. The coating is obtained by dissolving the compound in a volatile solvent (usually acetone) to give a solution of a definite concentration and pouring a known amount of this solution into the dish; the compound is uniformly distributed during the evaporation of the solvent by rotating and shaking (*fig. 1*). For tests on grain-weevils the bottom, walls and lid are treated, for flies only the lid. When the flies are attacked by the agent, they fall onto the untreated bottom; the dose which they have received from the lid must in itself be sufficient to kill (*fig. 2*).

#### *Resistance tests on flies*

As already mentioned, flies are now known that have become resistant to one or more insecticides; thus, wherever there has been intensive spraying with DDT, flies are found which are resistant to DDT. If such flies are treated with lindane — the gamma isomer of hexachlorocyclohexane (BHC) [7] — they very quickly die, but if the flies are treated with lindane for many generations without interruption, they likewise become resistant to this agent. In latter years we have cultured various resistant strains by regular spraying with a certain agent, so as to include them in our investigations.

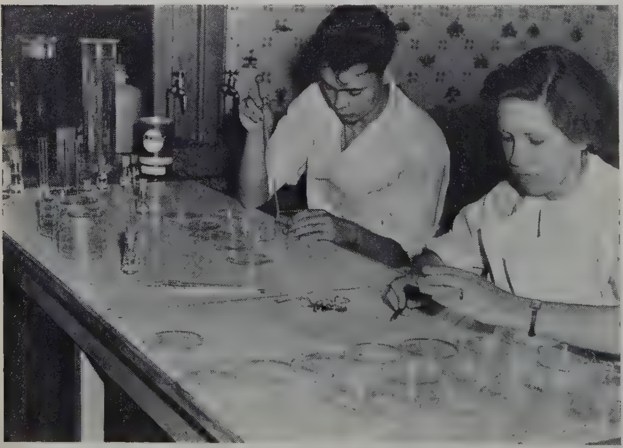

Fig. 1. Irrigation of petri dishes with a solution of the compound to be investigated for tests on flies and grain-weevils. The solvent (usually acetone) is allowed to evaporate, leaving behind a known quantity of the compound in a thin layer.

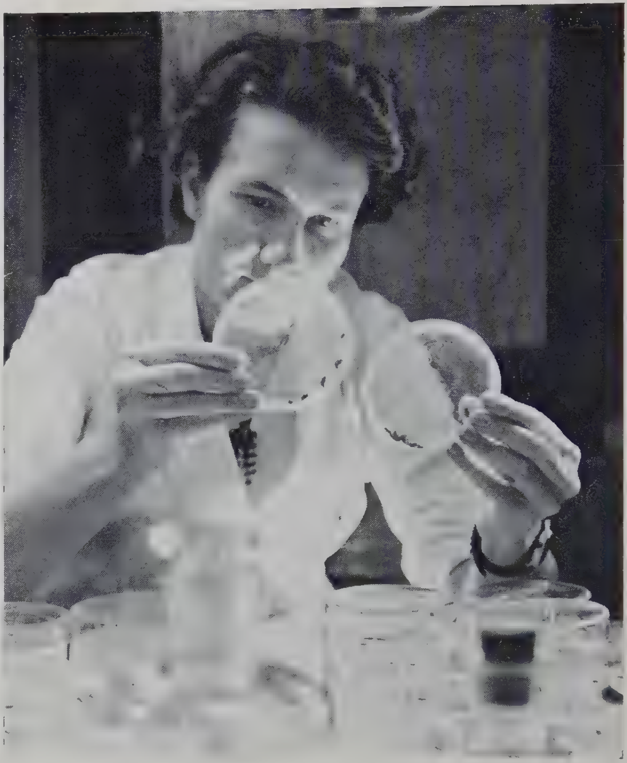

Fig. 2. Tests on flies in petri dishes that have been coated with lindane. The lindane has killed the strain of normal sensitivity (right) but has had no effect on the resistant strain (left).

As to the nature of resistance we are groping in the dark. Some investigators assume that resistance is based upon dechlorination of the compound in the body of the insect. This, however, has not yet been satisfactorily demonstrated.

In practice it is found that resistance by no means occurs in all species of insects; the behaviour of flies in this respect is the exception rather than the rule. Nor can flies be rendered resistant to all poisons. Thus, it has not so far been possible to impart resistance against phenyl N,N-dimethyl carbaminate [19] — provisionally designated as S 17 — although it is possible to render flies resistant to its chlorinated derivatives.

S 17 is not the only compound against which flies only become resistant with difficulty; their sensitivity to parathion and the pyrethrins, mentioned early in this article, does not depreciate significantly. Nevertheless none of these compounds are very suitable for controlling flies: parathion is far too toxic for use in houses and cow-sheds, and S 17 and pyrethrins have only a short active life. Latterly good results have been obtained against resistant flies with "Diazinone", a phosphorus compound of low toxicity.

For the time being, resistance can only be avoided by not using the same agent for too long a period at a stretch. Our laboratory experience has shown that it is desirable, even after only one spraying with DDT against flies in houses and cow-sheds, to transfer to another insecticide, since DDT will give rise to an appreciable resistance even in the first generation. Insecticides of the BHC group, such as lindane, are much more satisfactory; in their case resistance only occurs after several generations.

### *Tests on the potato root eelworm*

The dreaded "potato sickness" is caused by the potato root eelworm, a small worm about 0.5 mm in length (*fig. 3*). It lives in the roots of the potato plant and gives rise to a severe festering of some of the roots which develop gall-like growths. The latter interrupt the supply of food through the root, as a result of which the parts of the plant above ground wilt.

During the development of the female eelworm the abdomen greatly swells as it fills with eggs, and finally bursts out through the skin of the root. The spherical females can be seen as small knobbles on affected roots. When the female dies its body wall forms a tough envelope — the cyst, *fig. 4* — around the eggs and larvae. The larvae only make their appearance from the cyst when they come into contact with excretion product(s) of the potato root; that is, they are enticed from their lair only by one or more specific emergency stimulating substances. Should this not happen, the cysts remain virile in the ground for many years and thus constitute a serious threat to potato cultivation.

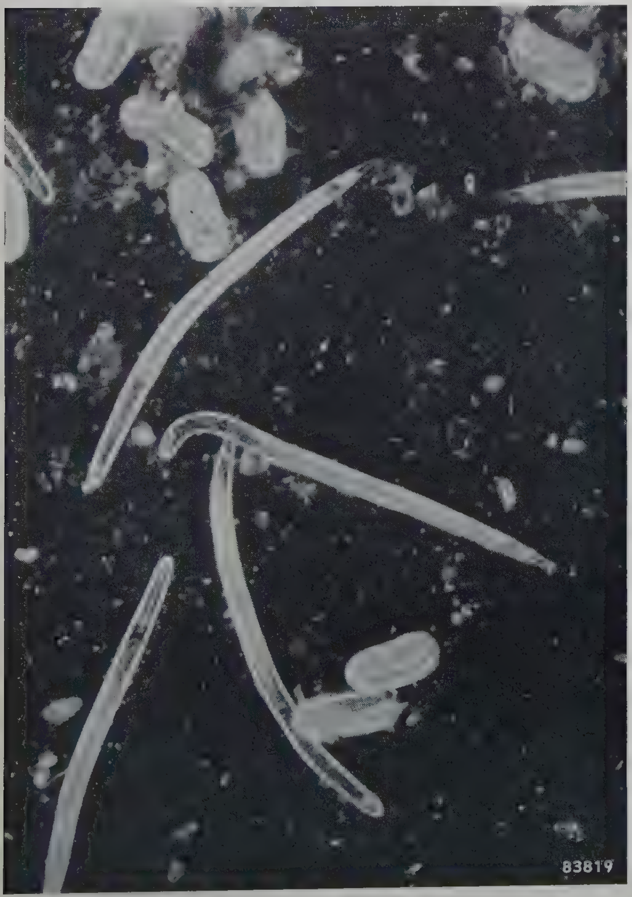

Fig. 3. Larvae and eggs of the potato root eelworm (*Heterodera rostochiensis*, Wollenw.), responsible for potato sickness. The larvae are about 0.5 mm long.

Fig. 4. Tube containing 10 000 cysts of the potato root eelworm (fig. 3).

In our tests, the cysts are exposed for a short while to the compounds to be investigated, washed and placed in plastic dishes. They are then put into water with which pots containing sand cultures of potatoes have been washed; this water contains the stimulating substance and activates the emergence of the larvae. The more active the combating agent the fewer the larvae leaving the cysts. The method is illustrated in *fig. 5*.

### **Tests on living plants**

Tests on leaf-devouring caterpillars and beetles, and on sap-sucking greenflies, thrips, spider mites etc., can only be carried out on living plants (*fig. 6*).

As previously remarked, it is the action of the residue left behind on the treated plant which especially interests us in the ectophytic agents. In our laboratory tests the treatment consists in immersing the plants in a solution, emulsion or suspension of the compound under review. When dry the plants are infected with the experimental animals.

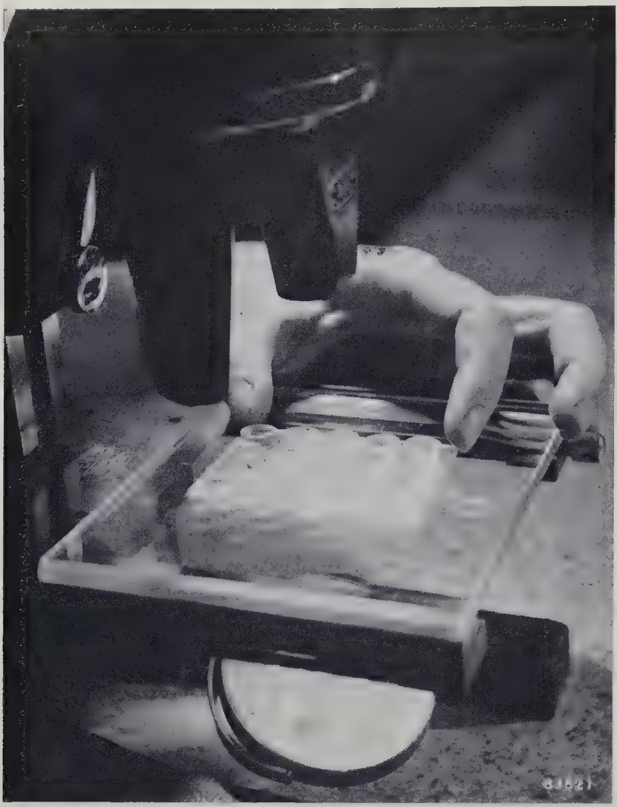

Fig. 5. With the aid of a binocular microscope it is ascertained whether a certain agent has been active against the eggs and the larvae of the potato root eelworm.

The normal arrangement for tests on caterpillars, beetles and greenflies may be seen in *fig. 7*. The plants infected with the insects are placed in glass cylinders, covered with gauze. Very small animals, such as thrips and spider mites, are applied to the leaf in small plastic boxes (*fig. 8*), so that they do not get lost.

The same arrangements are used in emphytic research; the only difference is that now the earth in the pot and not the plant is treated with the compound to be investigated. To exclude any possible action by the vapour from the compound the lower opening of the glass cylinders is carefully sealed with a plastic plate.

The rate at which the compound is transported through the plant can be studied by attaching the insect boxes (fig. 8) at various levels, and measuring how much later the one group is affected than the other. It can also be ascertained whether there is any transport from one leaf to the other or from the upper to the lower parts; for this purpose one leaf is treated with the emphytic agent and the boxes are attached at other suitably chosen positions.

### Follow-up investigations

When a material has passed the first test — i.e. has shown a lethal action towards the animal to be combated — the second phase of the research begins. This includes an accurate determination of the degree of activity on as great a number of animal species as possible, and an investigation of the behaviour of the compound under various conditions in which it is compared with known combating agents.

Of the many methods which can be applied here, we will name only those that give an insight into selectivity. When insects are injected with DDT

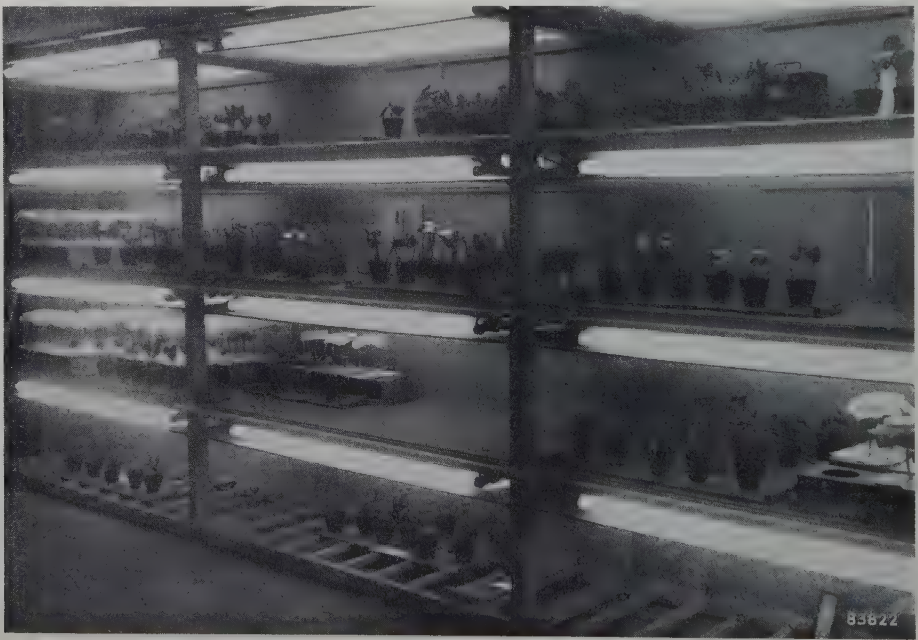

Fig. 6. Insect tests on living plants in an air-conditioned room.

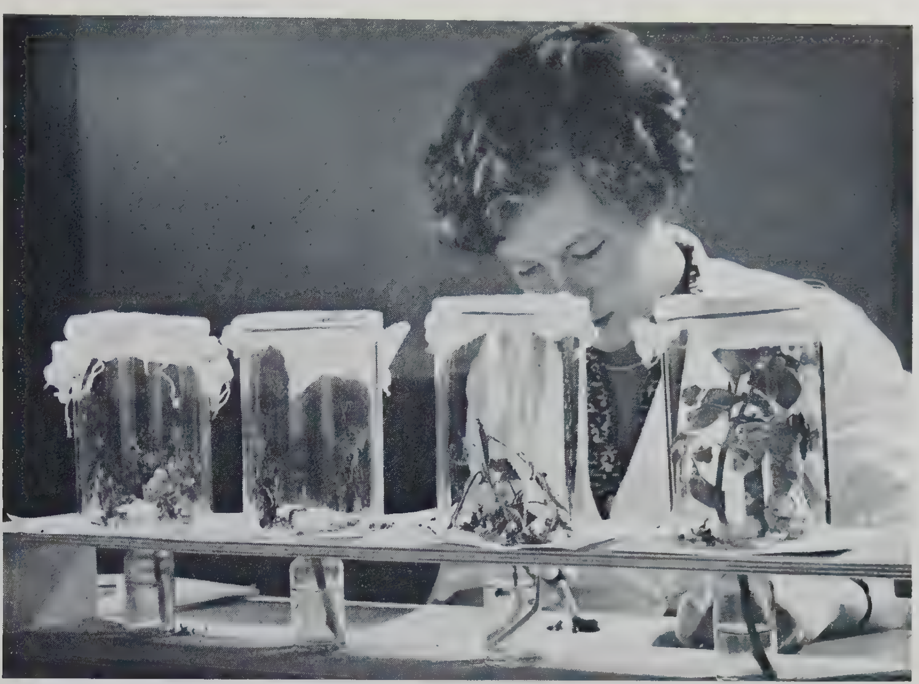

Fig. 7. Testing colorado beetle larvae on potato foliage in glass cylinders.

(*fig. 9*) and warm-blooded animals are given DDT by intravenous injection, the toxic doses per kilogram of living weight are found to be the same. But if DDT is brought into contact with the skin it is found that warm-blooded animals are relatively insensitive, compared with those insects that are sensitive to DDT. It is almost self-evident that for insects themselves there is likewise a difference in reaction time on injection or on contact with the skin. The two values thus found measure the toxicity and the rate of penetration respectively. The injection tests supply a more general value for the toxicity and from this value in combination with the contact toxicity an idea of the insecticidal value can be

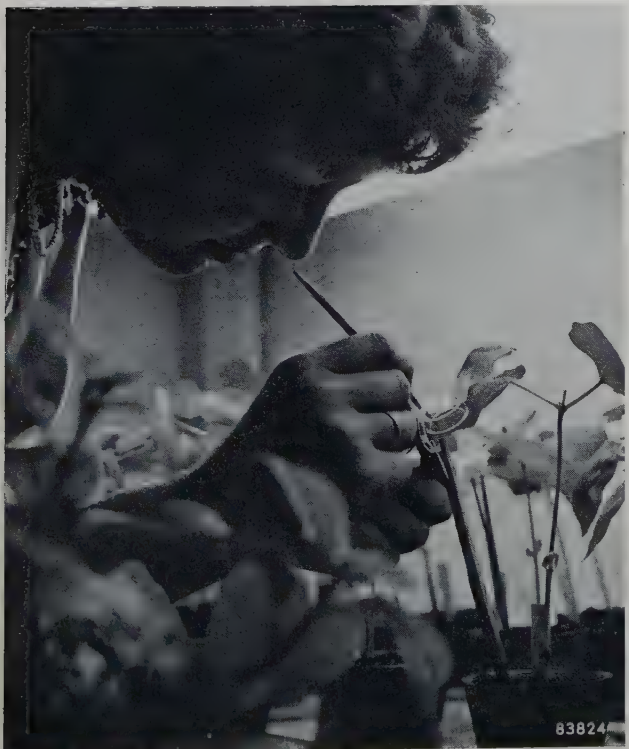

Fig. 8. Bean plants infected with spider mites. The latter are enclosed in a small plastic box.

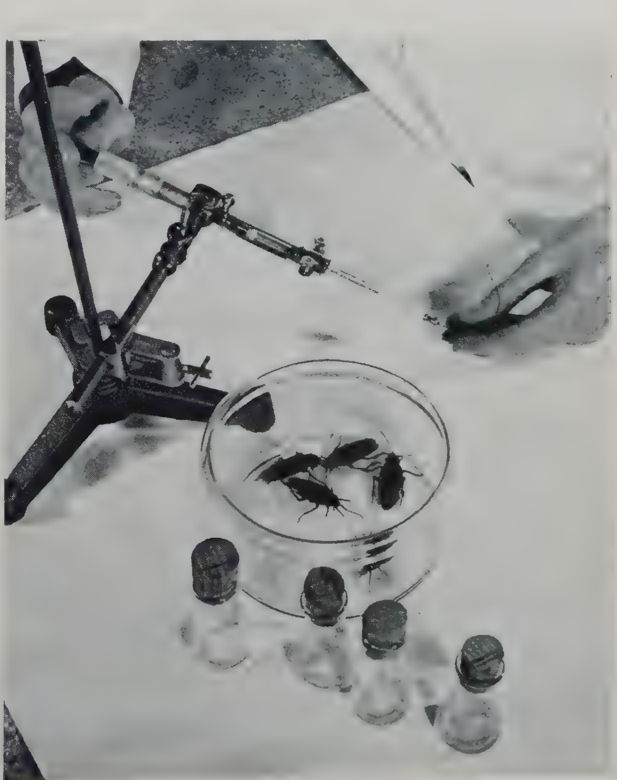

Fig. 9. Cockroaches injected with an insecticide by means of a micro-syringe.

obtained. Some idea can also be gleaned about the rate of penetration, but it should be remembered that little is known of the fate of insecticides within the body of insects. Once the second phase has passed off satisfactorily, there follows a third, in which the compound is tested in the field after its possible toxicity to warm-blooded animals has been determined. This will form the subject of a subsequent article.

### A new agent for combating the spider mite ("Tedion V 18")

Around the turn of the century, "fruit tree carbolineum" was used very extensively in fruit growing against insect eggs. It is not active against spider mite eggs. As a consequence the spider mite became an ever more serious pest ("fruit-tree red spider"). No adequate means was known for combating the spider mite. At first it was thought that a suitable agent had been found in parathion, but in practice it was not always satisfactory. True, the emphytic agent schradan [12] is most effective, but is unattractive because of its toxicity. In later years specific agents have been developed against the spider mite (acaricides) which are practically non-toxic to man. The most important are p-chlorophenylbenzene sulphonate [20], known as CPBS or PCPBS, and p-chlorobenzyl sulphide [21], known as chloroparacide.

Some years ago we were investigating a series of sulphones. They caused no mortality worth noting either with insects, spider mites or the eggs of the flour-moth. When later we examined these compounds for their action on spider mite eggs it turned out, much to our surprise, that they were active. The most active was 2,4,5,4′-tetrachlorodiphenyl sulphone [22], which was provisionally designated as V 18. It is remarkable that only the growing stages of the mites (eggs, larvae and nymphae [4])) are killed; V 18 has no more effect on mature mites than it has on insects. It is poisonous neither to plants nor to warm-blooded animals: for mice 5 grams of V 18 per kilogram of living weight produces not a single symptom of poisoning. Assuming that mouse and man are about equally sensitive, this would mean that a man weighing 70 kilograms could safely consume 350 grams of V 18. When it is considered that in our experiments a solution of only one part of V 18 in a million parts of spraying solution is often able to bring about total extermination of spider mite eggs and larvae, it will be seen that it is not only remarkably selective but also extremely active. It is in fact more active than the compounds just mentioned ([20] and [21]) and has the additional advantage that the risk of damaging the foliage is appreciably smaller.

The manufacture of V 18 will begin this year. It will be marketed under the name "Tedion V 18".

### APPENDIX: STRUCTURAL FORMULAE

Below are given the structural formulae of the compounds mentioned in the text.

[6] DDT . . . . . . . . .

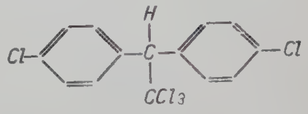

[7] HCH . . . . . . . . . . . .

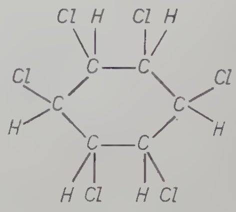

[10] Parathion . . . . . . . .

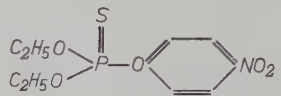

[12] Schradan . . . . . . .

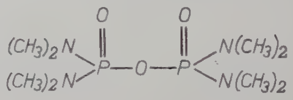

]19] S 17 . . . . . . . . . .

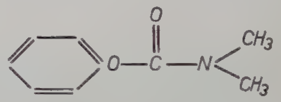

[20] CPBS . . . . . . .

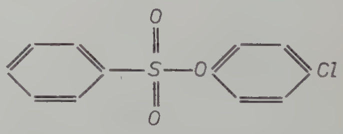

[21] Chloroparacide . .

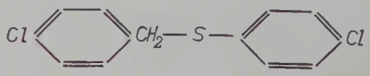

[22] „Tedion V 18" . .

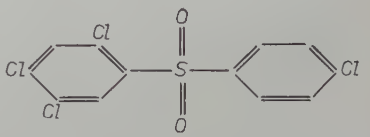

**Summary.** Pests injurious to cultivated plants are primarily of the insects species. After a historical survey of the development of insecticides — classifiable as stomach poisons and contact poisions — there is some discussion of "emphytic" (systemic) agents which render the plant itself poisonous to certain insects and consequently have many advantages over "ectophytic" agents.

From the work of the Boekesteyn laboratory in the search for pest control agents for animal pests, reports are given of: 1) resistance tests on flies, 2) tests on the potato root eelworm responsible for potato sickness, and 3) a new, highly specific agent against spider mite, harmless to man and domestic animals. This acaricide will be marketed under the name "Tedion V 18". In follow-up investigations, both contact tests and injection tests are made with the investigated compounds. The structural formulae of some of the compounds discussed are given in an appendix.

---

[4] A nymph is a stage intermediate between the larva and the adult and in appearance has already assumed great similarity to the latter.

# THE GLOSS POINT OF GLAZES

by R. W. P. de VRIES.

666.291.22:536.421.2.08

*With the development of glass manufacture and glass processing from an art into a science, objective methods of characterizing and identifying the behaviour of glass have gained ground in this branch of industry. Such developments have perhaps lagged somewhat behind as regards glazes and enamels.*

In glass working, just as in metal working, specific temperatures should be strictly adhered to, in order that the glass will have the physical properties required. As regards the types of glass from which the envelopes of lamps, radio tubes, X-ray tubes etc. are made, it is above all the viscosity that determines the requisite temperature for each of the different stages in the production process; it also frequently sets an upper limit to the temperature at which the product can safely be used. To characterize such a type of glass, therefore, not only are the coefficient of expansion and certain other important properties indicated, but also the temperature at which the viscosity possesses the specific values required for the various phases of manufacture; see *fig. 1.*

Away from the glasses used for blowing and working into bulbs, tubes, etc., there is another group, about which much less is known, viz. the glazes and enamels, for coating ceramics, glass and metals. The object may be to form a joint, or to provide a protective or decorative finish. The coating is effected by applying to the object a thin layer of a suspension of finely-ground glaze in water [1]. The layer is dried and the remaining grainy coating is fired in a furnace until fusion takes place. As soon as the object reaches a certain temperature during the firing process, the surface undergoes a fairly sudden transition from dull to bright. This temperature is termed the gloss point.

For the comparison of glazes, the viscosity curve discussed above is of little use. In the first place, the phenomenon in question, namely the smoothing out of the surface is not a unique function of the viscosity. The surface tension also has an effect and the time factor too plays a part. In the second place, the viscosity values of glaze glasses at the temperatures of firing are relatively low and for this reason they are more difficult to determine.

The appropriate method therefore is to ascertain the gloss point of the glaze direct from a firing test. This can be done during firing by observing the glaze through a viewing-aperture in the furnace wall and by noting the temperature at which the surface of the glaze is seen to become reflective by the light radiated from the walls inside the furnace, or (at temperatures below 700 °C) by the light supplied by an incandescent lamp.

When visually determining the gloss point in this way, it was found that there was sometimes an unaccountable spread in the results. To trace the cause of this, an arrangement was set up for

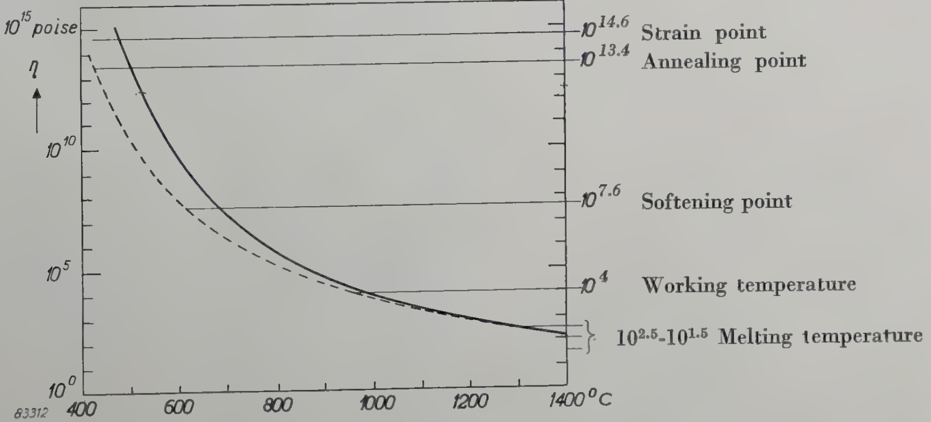

Fig. 1. The viscosity $\eta$ (in poise) of two types of glass as a function of the temperature. The full curve applies to soda glass, the dashed curve to lead glass. For processing, certain values of $\eta$ are required, which thus determine the processing temperatures.

---

[1] Physico-chemically there is no difference between glazes and enamels. For convenience we shall therefore speak henceforth only of glazes. A detailed account of these substances and of enamelling technique is given by L. Vielhaber, Emailtechnik, V.D.I., Düsseldorf 1953.

ascertaining the gloss point more objectively.

The basic layout is shown diagrammatically in *fig. 2*. A sample of the glaze is placed on a slide and heated in a small furnace. A beam of light is directed upon the sample through an opening in the furnace, and the light reflected from the sample emerges through a second opening and falls on a photo-electric cell. Initially, the sample reflects diffusely and the photo-electric cell therefore receives only a faint gleam. However, as soon as the gloss point is reached, the sample reflects almost as a mirror surface. The configuration of source, sample and photo-cell is so chosen that the reflected beam of light falls on the cell, which therefore now indicates a much higher luminous intensity. If the furnace temperature is gradually raised and the photo-electric current is plotted as a function of the temperature on an $X$-$Y$ recorder, the resultant curve will show a sharp upward step when the gloss point is reached. The special furnace is shown in *fig. 3* and the complete apparatus in *fig. 4*.

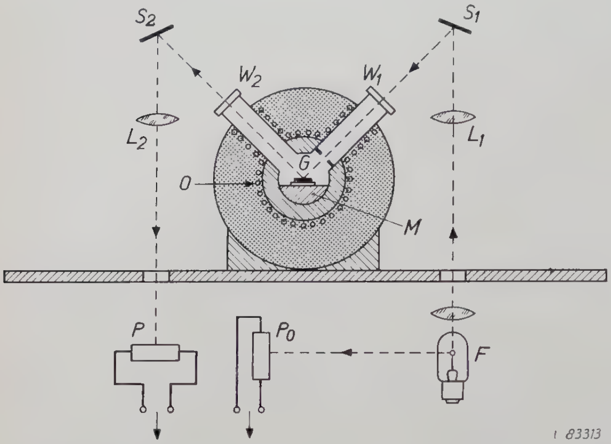

Fig. 2. Basic layout for the objective determination of the gloss point. In the furnace $O$ the sample $G$ is placed on a chrome-iron block $M$. By means of a small incandescent lamp $F$, lens $L_1$ and mirror $S_1$, a narrow beam of light is directed through window $W_1$ on to the glaze. Specularly reflected light leaves the furnace via window $W_2$ and is directed upon photo-electric cell $P$ by mirror $S_2$ and lens $L_2$. Direct light from the light source falls upon the photo-electric cell $P_0$. The ratio of the photo-electric currents from $P$ and $P_0$ is recorded as a function of the furnace temperature.

The measuring procedure is subject to a number of difficulties. The luminous intensity of the light source may vary during the recording of a curve. These variations are compensated by allowing a direct beam of light from the source to fall on a second, similar photo-electric cell and recording the ratio of the two photo-electric currents (reflected light/direct light) on the $X$-$Y$ recorder. A more serious difficulty is the radiation from the furnace which causes heating of the photo-electric cells. To minimize this effect, a type of selenium-cell with a small temperature effect is used and the cells are positioned lower than the furnace by deflecting the path of the light as shown in fig. 2. Moreover the furnace is so constructed that it works with a minimum of power, and its radiation is therefore kept to a minimum. The slide that carries the glaze sample must contribute as little reflected light as possible. At temperatures above approx. 600 °C the measurement becomes inevitable unreliable owing to the amount of light radiated by the slide and the inner walls of the furnace. This interfering effect can be avoided by using an intermittent light source and measuring only the synchronously varying part of the light received by the photo-electric cell; at present, however, our tests have not gone beyond 600 °C. It is of course important for the temperature of the sample at every instant to be defined and known with sufficient accuracy. This is not so easy to realize as it seems; a considerable loss of heat occurs through the opening near the sample, and it is consequently difficult to obtain a zone around the sample of sufficiently uniform temperature. Again, while the temperature is being raised, the sample temperature may wholly or in part lag a little behind that at the point of measurement (the location of the thermo-element used). In view of the importance of the rate of heating, as mentioned earlier, it is necessary to use a standardized heating curve in order to arrive at reproducible results. This is best done by automatic

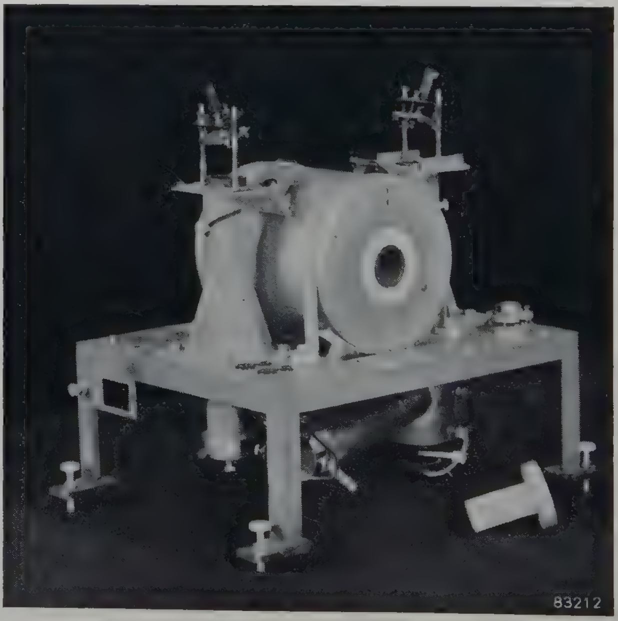

Fig. 3. Photograph of the apparatus sketched in fig. 2. The components marked in fig. 2 are easily identified. A spirit level can be seen on the right of the base plate of the furnace; the slide carrying the glaze sample must lie horizontally so that the glaze will not move out of the beam of light during the test.

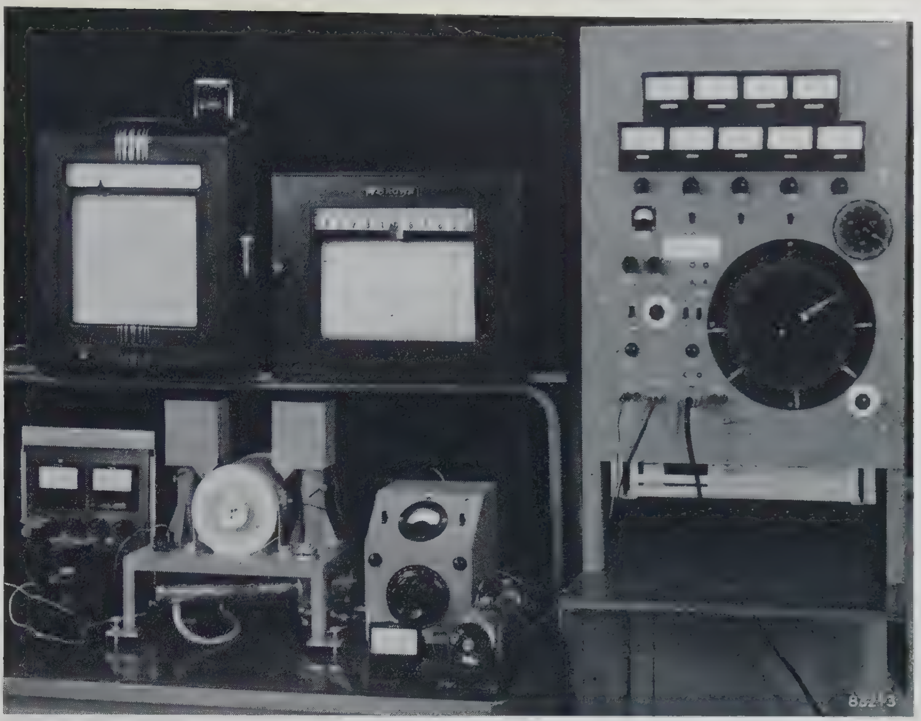

Fig. 4. Complete arrangement for the objective determination of the gloss point. Top left is the $X$-$Y$ recorder, and beside it an instrument which records the temperature as a function of time (for checking the heating-rate of the furnace; see fig. 7). Below the recorders is the furnace, with meters on either side giving direct indications of the separate photo-electric currents and the temperature and for adjusting the furnace power. At the right is the programming apparatus for controlling the furnace temperature.

programme control of the furnace. Finally, the preparation of the sample should be standardized too, since variations in grain size, grain distribution and packing can also influence the measurements.

So much attention is normally paid to the latter factors, which are of course equally important in the visual determination of the gloss point, that the cause of the spread in results mentioned above must be sought elsewhere. The explanation of the spread indeed soon became apparent from the curves recorded with the apparatus described. We shall now discuss some of these curves.

The curve in *fig. 5* was obtained for a jointing glaze. With its curious dip at the beginning of fusion, i.e. just below the gloss point, it was found very readily reproducible. Because of this reproducibility, it was possible to break off the firing of different samples at various points in the critical temperature range in order to find out what appearance of the glaze surface corresponded to the various points on the curve. Some photographs of such samples are shown in *fig. 6;* they correspond to points $I$-$V$ in fig. 5. At point $I$ the sintering has only just started (the grains can no longer be blown from the slide). At point $IV$ the surface has not yet become fully bright, whereas at point $V$ the gloss point has evidently been well exceeded. The visually determined gloss point was found to lie at point $g$; with this glaze the visual determinations were fairly consistent.

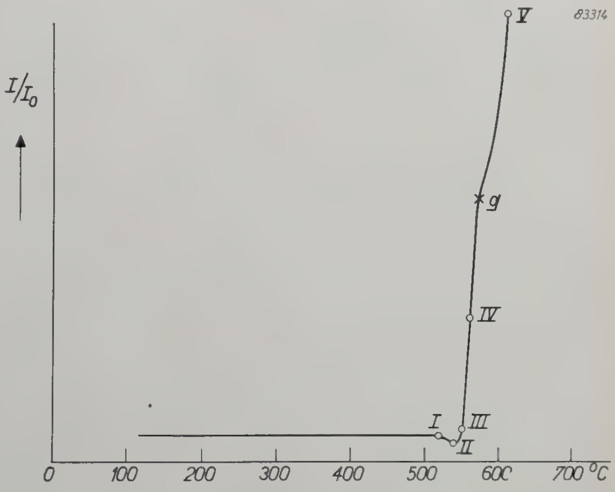

Fig. 5. Recorded gloss curve of a jointing glaze. The ratio $I/I_0$ of specularly-reflected light to incident light is recorded as a function of the temperature. The test, carried out on a number of samples, was broken off at various points of the curve ($I$-$V$), by quickly removing the sample from the furnace. The sudden increase in viscosity, due to rapid cooling, "freezes" the surface appearance of the sample, so that it can be inspected at room temperature. Point g can be regarded as the gloss point.

Comparing sample *I* and sample *II* under the microscope, it was found that at point *II* of the curve the grains were just becoming rounded off at the beginning of fusion (grains sticking together) whereas this had not yet started at point *I*. The dip at point *II* can now be explained by the fact that after entering a grain the light has to travel further in the glaze before leaving it again due to scattering. Owing to absorption in the glaze it will have become attenuated, so that the measured reflection which is still diffuse, is somewhat reduced.

*Fig. 7* shows the much more complicated curve plotted for an experimental glaze, consisting mainly of boron oxide (10%) and lead oxide (85%). Here too the dip is obtained just before fusion. The further great fluctuations in the reflection from the sample can be related to the physico-chemical behaviour as follows: after the glaze has fused to a glossy layer, it begins, at a somewhat higher temperature, to deglaze (crystallize) and therefore to assume a dull appearance again. When the temperature is raised still higher, the minute crystals that have been formed either fuse again or dissolve in the residual glass mass. A moment later, the mass deglazes once more, after which final and real fusion takes place. It is hardly surprising that this chain of events gives conflicting results in the visual determination of the gloss point. An observer who conscientiously records the very first signs of brightening has the best chance of arriving at a reproducible result — but the mere reproducibility of this particular result is of little consequence; the important thing is to recognize the deglazing effects, since it is upon these that the glaze will have to be rejected for most applications.

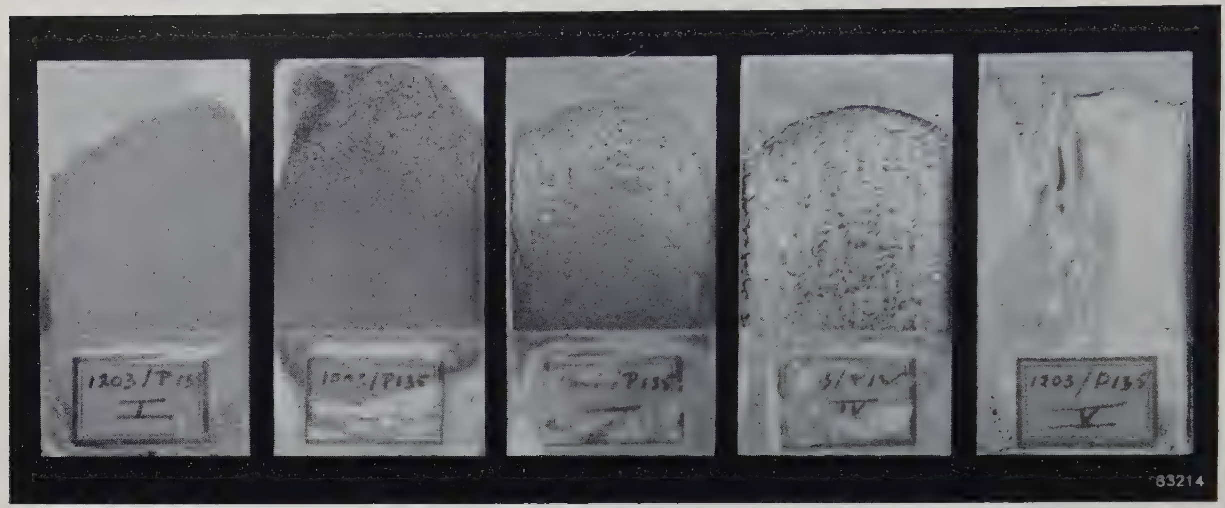

Fig. 6. Photographs of glaze samples, heated to points *I-V* indicated in fig. 5.
*I*: The grains of glaze powder have only just started to adhere to the underlayer: very first signs of sintering.
*II*: Grains rounded off, beginning of fusion.
*III*: First signs of specular reflection in the hollows between the grains.
*IV*: Whole surface not yet completely bright.
*V*: Completely bright surface; the gloss point (*g*) has been well exceeded.

Again, the curve in fig. 7 was found to be readily reproducible. It was therefore again possible to break off the firing process at certain points of the curve in order to confirm the deglazing effects by means of X-ray diffraction analysis. Analyses were carried out for points *IV*, *V* and *VI* of the curve in fig. 7.

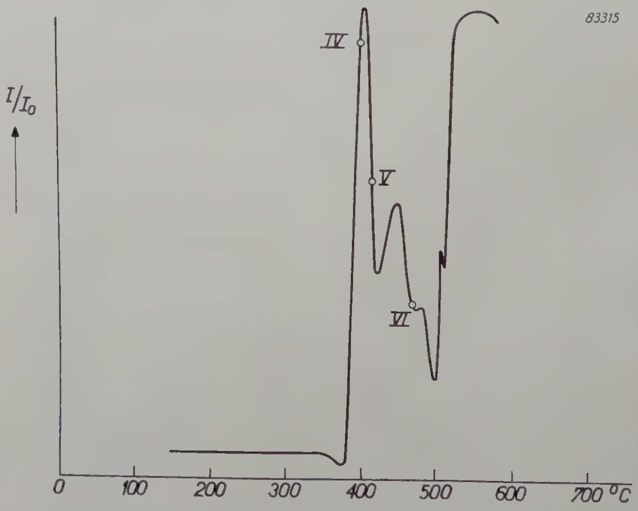

Fig. 7. Recorded gloss curve of an experimental glaze prepared in the laboratory. The heating-rate was 2 °C per minute. As the heating-rate increased, the curve was displaced as a whole towards somewhat higher temperatures without appreciable changes in the various features of the curve.

For point *IV* only a glass phase was found (no sharp diffraction lines); for point *V* the preparation was found to have, in addition to the glass phase, a crystalline phase of $\beta$-$Pb_4B_2O_7$; in point *VI* this crystalline phase had disappeared and in its place were identified crystals of $\alpha$-$PbB_2O_4$. In this way confirmation was found for the deglazing as such, and for the difference between the two deglazing processes.

As the foregoing clearly shows, the objective determination of the gloss point can be a valuable means of investigating and, eventually perhaps, of mastering the composite physico-chemical processes that take place during the firing of glaze powders.

**Summary.** When firing a layer of glaze powder on a slide in a small furnace it is found that at a certain temperature the surface of the layer undergoes a sudden transition from dull to bright. The conventional visual determination of this "gloss point" on some glazes prepared and tested in the laboratory produced widely varying results. For this reason an objective method of determining the gloss point was developed, whereby two photo-electric cells are used in conjunction with an *X-Y* recorder, which plots the degree of specular reflection obtained against the temperature of the glaze. The resulting curves were found to be readily reproducible. In some cases they are of complicated form, which makes the non-reproducibility of the visual determinations understandable; in the course of further investigations it was possible to relate various features of the curves to deglazing effects.

---

# ABSTRACTS OF RECENT SCIENTIFIC PUBLICATIONS OF N.V. PHILIPS' GLOEILAMPENFABRIEKEN

Reprints of these papers not marked with an asterisk * can be obtained free of charge upon application to the Administration of the Philips Research Laboratory, Eindhoven, Netherlands.

**2190:** W. J. Oosterkamp and T. Tol: Prinzipielle und praktische Grenzen der Detailerkennbarkeit bei verschiedenen röntgenologischen Beobachtungsmethoden insbesondere bei Verwendung der Bildverstärkerröhre (Fort. Röntgenstr. Röntgenpraxis **81**, 381-392, 1954, No. 3). (Theoretical and practical limits of etdila perception in various radiological techniques, in particular, using the image intensifier: in German).

The theoretical limit of the detail perceptibility in fluoroscopy with and without image intensifier, in full size normal radiography, miniature radiography and in intensifier radiography, is determined by the fluctuations of the number of quanta or particles conveying the information during the different stages of the radiological process. This theoretical limit is calculated on the basis of a measurement of these numbers of quanta. Every X-ray quantum absorbed in the primary fluorescent screen contributes to the visual impression when the image intensifier is used. This is not the case in normal fluoroscopy and miniature radiography, where only 1% of the absorbed X-ray quanta are effective.

The observed detail perceptibility is limited by the fluctuations of the X-ray quanta for intensifier fluoroscopy at low X-ray intensities and for intensifier radiography with very sensitive emulsions and large apertures; X-ray quanta fluctuations and instrumental deficiencies (lack of definition and loss of contrast) have approximately the same influences in the case of intensifier radiography on fine grain emulsions; the instrumental deficiencies are predominant in miniature radiography and in full size radiography (with intensifier screens).

The X-ray dose is 70-300 times smaller in intensifier radiography as compared with miniature radiography if the same emulsion is used, the detail perceptibility being approximately the same. The detail perceptibility of the intensifier radiograph on a fine grain 35 mm film approaches that of the full-size radiograph; only half the dose is necessary in the former case.

**2191:** H. Bremmer: The extension of Sommerfeld's formula for the propagation of radio waves over a flat earth, to different conductivities of the soil (Physica **20**, 441-460, 1954).

The influence of non-homogeneous soil conditions on the propagation of radio waves over a flat earth can be investigated with the aid of an integral equation based on Green's theorem. This equation applies to all types of distributions (also continuous) of the conductivity and of the dielectric constant of the earth; it is comparable with the integral equation considered by Hufford for the propagation over irregular terrain. The special solution for two adjacent regions of homogeneous electrical constants can be treated numerically with the aid of two different expansions for the field near the separating boundary and for the field far beyond this boundary; the rigorous solution of the integral equation proves to be identical with the corresponding expression derived in a very different way by Clemmow. The solution for three adjacent homogeneous regions can be obtained by solving the general eqation by a similar method.

**2192:** C. J. Bouwkamp and H. B. G. Casimir: On multipole expansions in the theory of electromagnetic radiation (Physica **20**, 539-554, 1954).

A new method is developed for expanding the electromagnetic field of radiating charges and currents in multipole components. Outside a sphere enclosing all sources the field is represented in terms of two scalar wave functions (Debye potentials) which are expanded in Legendre and spherical Bessel functions. The various terms of these series expansions are shown to be closely related to the radial components of the electric and magnetic vectors and hence determine at once the various multipole terms of the radiation field. It is emphasized that an alternative method based on the conventional vector-potential presentation has several disadvantages. The authors avoid the use of group theory and tensor calculus and apply only ordinary vector calculus. Attention is drawn to some simple source representations of the radial field components.

**2193:** T. Tol and W. J. Oosterkamp: Visibility of X-ray quantum fluctuations on image intensifier radiography (Nature **174**, 397-398, 1954).

The gain in brightness in radiography with an X-ray image intensifier is accompanied by a visual "noise" effect, especially at low X-ray intensities and high intensification factor. Its origin lies in quantum fluctuations and the spatial distribution of the grain clusters of the photographic emulsion, each effective photon being responsible for the appearance, after development, of a cluster. Photographs illustrating the effect are shown. See also Philips tech. Rev. **17**, 75-76, 1955/56.

**2194:** F. J. Mulder: Simplified isolation of the nonsaponifiable matter in the analysis of oils (Rec. Trav. chim. Pays-Bas **73**, 626-628, 1954, No. 8).

A simplified method is given for the analytical isolation of non-saponifiable matter from oils. After saponification in alcohol the alcoholic soap solution is completely dissolved in a measured quantity of benzene and the benzene solution is washed with water. The concentration in the benzene solution is determined after drying. By this method the tedious operations of extraction and quantitative transfer of the extracts are avoided. This method is suitable for the determination of the vitamins A and D.

**2195:** F. de Boer and W. F. Niklas: Application of a tracer to cathode-gettering and gas-adsorption problems (Brit. J. appl. Phys. **5**, 341-342, 1954, No. 9).

The residual gas pressure in a cathode-ray tube decreases when the cathode is heated. It is conjunctured that absorption by the barium-strontium oxide layer on the cathode is responsible. This absorption has been demonstrated by admitting into a cathode-ray tube some $CO_2$ containing a trace of $C^{14}$, and subsequently measuring the radioactivity of the cathode. In addition, it has been established that the gas absorption of other components of the electron gun is about 500 × less than that of the oxide layer on the cathode.

**2196:** F. de Jager: Les limites théoriques de la transmission en cas de niveau de bruit élévé, pour differents systèmes de modulation continue et de modulation codée (Onde electrique **34**, 675-682, 1954, Nos. 329-330).

The signal-to-noise ratio is examined for systems of frequency modulation, pulse position modulation, pulse code modulation (binary code) and delta modulation, in particular at high noise levels. In choosing the value of the optimum passband, a theoretical limit for the signal-to-noise ratio is found which is roughly equal for all the systems. To obtain, for example, a signal-to-noise ratio of 30 dB, the minimum power for each system must be 17 dB higher than the power of the noise found in a passband corresponding to the original signal. To get a signal-to-noise ratio of 40 dB, the corresponding figure is 20 dB. Finally the theoretical limits of the signal-to-noise ratio are examined for transmission in a chain of 50 links.

**2197:** H. G. Beljers, L. van der Kint and J. S. van Wieringen: Overhauser effect in a free radical (Phys. Rev. **95**, 1683, 1954, No. 6).

If a paramagnetic substance is placed in a magnetic field and electron spin resonance is excited by a microwave field, the thermal equilibrium of the electron spin system is disturbed. According to Overhauser, nuclear spins, if present, are aligned by relaxation processes which try to restore equilibrium. The above experiment has been performed using the free radical diphenyl picryl hydrazyl (DPPH) in a magnetic field of 3300 Oe. A microwave field of 3.2 cm wavelength gave resonance absorption approaching saturation. Alignment of the protons in the DPPH is observed by a considerable increase of the proton resonance at 14 Mc/s.

**2198*:** F. A. Kröger and H. J. Vink: Die Regulierung von elektrischen und optischen Eigenschaften von polaren kristallen (Contribution to Halbleiterprobleme I, edited by W. Schottky, Vieweg, Braunschweig 1954). (The control of electric and optical properties of polar crystals; in German).

This article contains the more important results of an investigation which is reported in detail in Z. phys. Chem. **203**, 1-72, 1954, Nos 1-2 (see these abstracts No. **2180**).

**R 249:** E. W. Gorter: Saturation magnetization and crystal chemistry of ferrimagnetic oxides, Part II (Philips Res. Rep. **9**, 321-365, 1954, No. 5).

Continuation of *R 248*. Néel's theory is reviewed in section 2.2.1, with Yafet and Kittel's modification (section 2.2.2). When the moments of the two sublattices are approximately equal, Néel predicts a number of anomalous $\sigma$—$T$ curves. All of these should occur in a series of mixed crystals of type (a) in which the resultant moment $m$ changes sign. Our experimental methods are given in section 3. The measurements on the single ferrites $\mathrm{Me^{II}Fe_2^{III}O_4}$, with $\mathrm{Me^{II}} = \mathrm{Mn^{2+}}, \mathrm{Fe^{2+}}, \mathrm{Co^{2+}}, \mathrm{Ni^{2+}}, \mathrm{Cu^{2+}}, \mathrm{Mg^{2+}}$ or $(0.5\ \mathrm{Li^+} + 0{\cdot}5\ \mathrm{Fe^{3+}})$ show that these belong to group (a); the mixed crystals $\mathrm{Me_{1-a}Zn_aFe_2O_4}$ with $a >$ appr. 0.4 belong to group (b) (section 4). The moment of $\mathrm{Ca_{0.35}\ Zn_{0.65}Fe_2O_4}$ is higher than that of any MgZn ferrite, perhaps because the angle *A*-O-*B* is increased by the presence of the greater part of the large Ca ions in the *B* sites, thus increasing the *AB* interaction; this behaviour would be in agreement with Anderson's theory (section 5.1; Anderson's theory is reviewed in section 2.3.2). The moments of ferrimagnetic oxides with other crystal structures may be predicted from the angles (metal ion) - ($\mathrm{O^{2-}}$ ion) - (metal ion); cf. $\mathrm{BaFe^{III}_{12}O_{19}}$ and $\mathrm{KFe^{III}_{11}O_{17}}$ (section 5.2).

**R 250:** G. Brouwer: A general asymptotic solution of reaction equations common in solid-state chemistry (Philips Res. Rep. **9**, 366-376, 1954, No. 5).

A theory of the chemistry of semiconductors, given recently by Kröger, Vink and Van den Boomgaard, is based on a number of reaction equations and certain additional conditions, including electroneutrality. A simple way to find an analytical or graphical approximate solution of this set of equations is presented in this report. Two examples are given; the method, however, is not restricted to these systems. The accuracy of the method is quite sufficient to serve its purpose.

**R 251:** H. A. Klasens: Temperature dependence of the luminescence and chemical stability of basic magnesium arsenate activated with tetravalent manganese (Philips Res. Rep. **9**, 377-390, 1954, No. 5).

The effect of activator concentration and partial substitution of the lattice constituents by other ions on the temperature dependence of the luminescence of $6\ \mathrm{MgO{\cdot}As_2O_5{\cdot}Mn}$ is studied. The effect of the activator concentration is in agreement with the theory of Johnson and Williams. Incorporation of lithium improves the temperature dependence considerably. Measurements of the stability of various arsenates in reducing atmospheres show that phosphors containing lithium are less easily reduced. Incorporation of fluorine has the opposite effect. A theory for this induced variation of stability is given.

**R 252:** J. L. H. Jonker: The similarity law of secondary emission (Philips Res. Rep. **9**, 391-402, 1954, No. 5).

In the literature, the curves of the secondary-emission coefficient $\delta$ measured as a function of the energy $\varepsilon V_\mathrm{p}$ of the primary electrons often show large deviations from the experimental universal curve, i.e. do not satisfy the similarity law. It is shown that some of these deviations may be caused by the fact that the target is partly or completely covered with foreign materials. Many materials have been re-measured with extra precautions to ensure a clean surface, and tables are given for a number of materials whose measured $\delta$ curve agreed with the experimental universal curve. In that case the indication of the values of $\delta$ and $\varepsilon V_\mathrm{p}$ at the maximum of the $\delta = f(\varepsilon V_\mathrm{p})$ curve is sufficient; other values of $\delta$ can then be deduced from the experimental universal curve, for which a formula is given.

**R 253:** E. W. Gorter: Saturation magnetization and crystal chemistry of ferrimagnetic oxides, Part III (Philips Res. Rep. **9**, 403-443, 1954, No. 6).

Continuation of R 248 and R 249. In a number of mixed-crystal series, anomalous $\sigma$-$T$ curves have been looked for: these are not found in the systems $Ni_{1+a}Fe^{III}{}_{2-2a}Ti_aO_4$ and $Ni_{1.5-a}Zn_aFe^{III}Ti_{0.5}O_4$ because of the unexpected presence of $Ti^{4+}$ ions in tetrahedral sites, proved for $Ni_{1.5}Fe^{III}Ti_{0.5}O_4$ by measurements of the effective *g*-factor (section 6.1.2). In the system $Li_{0.5}Fe^{III}{}_{2.5-a}Cr_aO_4$ ($0<a<2{\cdot}0$), the distribution of the $Li^+$ and $Fe^{3+}$ ions is anomalous as a result of short-range order. The resultant moment remains positive, and only one type of anomalous $\sigma$-$T$ curve, viz. that for which the spontaneous magnetization changes sign with temperature, occurs in a wide range of compositions. For $a \leqslant 1.25$ the materials belong to group (a) (section 7). A change of sign of the resultant moment does occur in the system $NiFe^{III}{}_{2-a}Al_aO_4$. Anomalous $\sigma$-$T$ curves are here found in a narrow range of compositions, but not all types predicted by Néel: the reasons are discussed (section 8). The presence of $Mn^{2+}$ ions apparently promotes the formation of angles between the ionic moments in *B* sites: the complete system $MnFe^{III}{}_{2-a}Cr_aO_4$ belongs to group (b) (section 9), as well as $MnFe_2O_4$ prepared by other authors (section 4) and part of the system $Ni_{1.5-a}Mn_aFe^{III}Ti_{0.5}O_4$ (section 6.3). In the first-named system *m* probably changes sign only as a result of these angles.

**R 254:** P. Cornelius: Vorschläge betreffend die Einheiten der Fläche, der dielektrischen Verschiebung und der magnetischen Feldstärke (Philips Res. Rep. **9**, 444-457, 1954, No. 6).

Suggestions with regard to the definition of the units of dielectric displacement and magnetic field strength, to remove certains difficulties in connection with the retionalization of units.

**R 255:** A. Versnel and J. L. H. Jonker: A magnetless magnetron (Philips Res. Rep. **9**, 458-459, 1954, No. 6).

A description is given of an oscillator tube that behaves like a magnetron. A feature of the new tube is that no magnetic field is needed. Measurements are discussed also.

**R 256:** J. Smit and H. G. van Bueren: Elastic aftereffect in a-iron in relation to the elastic constants of cubic metals (Philips Res. Rep. **9**, 460-468, 1954, No. 6).

The elastic after-effect in $\alpha$-iron, containing carbon or nitrogen in solid solution, can be interpreted as causing a change of the elastic moduli of the material. This interpretation renders it possible to estimate with a reasonable degree of accuracy the magnitude of the after-effect in polycrystalline materials. The estimate is based on a general relation which is shown to exist between the elastic constants of single crystals and of polycrystalline specimens of the cubic metals.

**R 257:** Th. P. J. Botden, C. Z. van Doorn and Y. Haven: Luminescence of F-centres in alkalihalide crystals (Philips Res. Rep. **9**, 469-477, 1954, No. 6).

Crystals of KCl, KBr, KI, NaCl and RbCl coloured additively have been irradiated in the *F*-absorption band at liquid-hydrogen and liquid-nitrogen temperatures. In all crystals an infra-red luminescence has been observed between about 1 and 1·5 $\mu$. The luminescence is quenched at temperatures above 100-150 °K. The quantum efficiency is very low and the luminescence appears only when the crystals are kept at low temperatures after the formation of the *F*-centres and quenching in liquid nitrogen. Different results are obtained when the crystals are kept at room temperature in the dark or during irradiation. It is believed that the infra-red emission is to be attributed to *F*-centres.